Dielectric spectroscopy and conductivity of polyelectrolyte solutions

2004 J. Phys.: Condens. Matter 16 R1423

(http://iopscience.iop.org/0953-8984/16/49/R01)

INSTITUTE OF PHYSICS PUBLISHING JOURNAL OF PHYSICS: CONDENSED MATTER

J. Phys.: Condens. Matter **16** (2004) R1423–R1463 PII: S0953-8984(04)34390-0

TOPICAL REVIEW

Dielectric spectroscopy and conductivity of polyelectrolyte solutions

F Bordi[1], **C Cametti**[1] **and R H Colby**[2]

[1] Dipartimento di Fisica, Università di Roma 'La Sapienza' and Istituto Nazionale per la Fisica della Materia (INFM CRS_SOFT), Unità di Roma1, Italy
[2] Department of Material Science and Engineering, Pennsylvania State University, University Park, PA 16803, USA

Received 31 August 2004
Published 26 November 2004
Online at stacks.iop.org/JPhysCM/16/R1423
doi:10.1088/0953-8984/16/49/R01

Abstract

The dielectric and conductometric properties of aqueous polyelectrolyte solutions present a very complex phenomenology, not yet completely understood, differing from the properties of both neutral macromolecular solutions and of simple electrolytes. Three relaxations are evident in dielectric spectroscopy of aqueous polyelectrolyte solutions. Near 17 GHz, water molecules relax and hence this highest frequency relaxation gives information on the state of water in the solution. At lower frequencies in the MHz range, free counterions respond to the applied field and polarize on the scale of the correlation length. This intermediate frequency relaxation thus provides information about the effective charge on the polyelectrolyte chains, and the fraction of condensed counterions. However, the presence of polar side chains adds a further polarization mechanism that also contributes in this intermediate frequency range. At still lower frequencies, the condensed counterions polarize in a non-uniform way along the polyelectrolyte chain backbone and dielectric spectroscopy in the kHz range may determine the effective friction coefficient of condensed counterions. In this review, we analyse in detail the dielectric and conductometric behaviour of aqueous polyelectrolyte solutions in the light of recent scaling theories for polyelectrolyte conformation and summarize the state-of-the-art in this field.

1. Introduction

Although the dielectric method has been established for well over 100 years, it is still one of the most important techniques for studies of the structure and dynamics of polymer solutions. This is because it can investigate the relaxation processes occurring in aqueous polymer solutions in an extremely wide range of characteristic times, roughly from 10^{-12} to 10^{3} s [1–4].

The principles of measurement are very simple. The electrical impedance of an appropriate device containing the sample to be investigated is measured as a function of the frequency of the

applied electric field. However, various limitations have hampered the application of dielectric spectroscopy to aqueous polyelectrolyte solutions. There are three reasons for this. Firstly, the dielectric spectra generally extend from hertz to gigahertz frequencies, requiring diverse equipment to obtain comprehensive data for a given system and a rather sophisticated analysis of the data in order to separate the different contributions. Secondly, aqueous systems usually display a very high ionic electrical conductivity which causes a giant frequency-dependent dielectric dispersion, falling in the low-frequency tail of the spectrum that generally masks the relaxations associated with the polymer component. Thirdly, there is a strong polarization in the vicinity of the electrodes that can dwarf the relaxation of interest in the sample. In section 2 we describe the methods that have been developed to overcome these limitations.

Extensive reviews and whole books have been devoted to the properties of polyelectrolyte solutions [5–11] and no attempt is made here to provide a comprehensive review of the vast literature that exists on these subjects. The present work, aimed to a more limited and practical scope, is meant to demonstrate the application of dielectric spectroscopy to aqueous polyelectrolyte solutions, with the intent of gaining information, at a molecular level, on the peculiar behaviour of these systems. This review is organized as follows. After a brief phenomenological introduction of the dielectric parameters used to describe the electrical behaviour of aqueous polyelectrolyte solutions, we discuss the different experimental methods employed in dielectric measurements in section 2, focusing on the correction of the electrode polarization effect. Section 3 reviews simple ideas about counterion condensation and polyelectrolyte conformation in solution. In section 4 we analyse the different contributions to a typical dielectric spectrum of polyelectrolyte solutions in the frequency range between kHz and GHz. Finally, in section 5, we discuss the electric conductivity of these systems in the light of both counterion condensation theory and the scaling approach.

1.1. Dielectric spectra of polyelectrolyte solutions: general

The dielectric and conductometric spectra of aqueous polyelectrolyte solutions, extending over a wide frequency range, present a very complex shape, involving three or more different, partially overlapping, contributions, each of them originated by different molecular level mechanisms [7, 12]. They may be classified as due to polyion dipolar orientation relaxation, polarization of condensed counterions, polarization of the ionic atmosphere, long-range solvent-ordering effects and, at higher frequencies, to orientational polarization of the water molecules, possibly modified by the interaction with the solute.

Despite the variety of mechanisms involved in the dielectric response of aqueous polymer solutions, some general features emerge that are common to all polyelectrolyte solutions investigated to date. The dispersion region in the lower frequency range, typically around some tens of kilohertz, is characterized by a large dielectric increment, apparently arising from relaxation of condensed counterions along the polyion chain. This effect depends, in a rather complicated way, on the charge distribution along the chain, governed by the counterion condensation phenomena [5, 13, 14], occurring when the charge density on the polyion exceeds a critical value. This phenomenon is perhaps the most prominent feature of aqueous polyelectrolyte solutions and divides the counterions into two types. One type are ‘bound’ counterions which stay in the vicinity of the charged polymer and the other type are ‘free’ counterions which dissociate from the polymer chain, interacting through a screened Coulomb (Yukawa) potential:

$$\frac{U}{kT} = \frac{l_B}{r}\exp(-r/r_D). \tag{1}$$

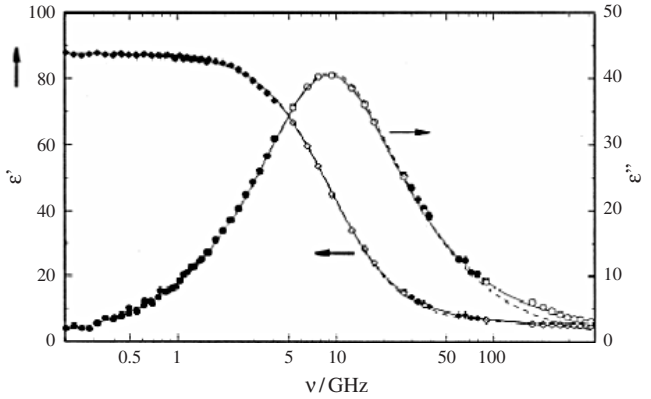

Figure 1. The dielectric dispersion of water at 0.2 °C [15]. The broken curve represents a single Debye relaxation and the solid curve a superposition of two Debye relaxations. At this temperature, the dielectric parameters that characterize the two dispersions are [15]: $\Delta\varepsilon_1 = 87.57$, $\nu_1 = 9.0$ GHz, $\Delta\varepsilon_2 = 6.69$, $\nu_2 = 177$ GHz and $\varepsilon_\infty = 3.92$. Usually, in dielectric investigations of polyelectrolyte aqueous solutions up to a few GHz, the dielectric dispersion of water is described by a single Debye relaxation or, more precisely, by a Cole–Cole relaxation function with a relaxation-time spread parameter close to unity ($\alpha \approx 0.98$, see figure 8) (in this case, see appendix for the evaluation of the parameters of relaxation).

This equation applies for univalent counterions interacting with each other at separation r, where

$$l_B = \frac{e^2}{\epsilon kT} \tag{2}$$

is the Bjerrum length (e is the elementary charge and ϵ is the dielectric constant of the solvent medium) $l_B = 7.12$ Å at 20 °C in water and

$$r_D = \left(4\pi l_B \sum_i c_i\right)^{-1/2} \tag{3}$$

is the Debye screening length. The sum in equation (3) is generally taken over all small free ions present at concentration c_i (dissociated 'free' counterions and any added salt ions).

The dispersion at high frequency, around some tens of gigahertz, is attributed to the orientational polarization of water molecules [1, 2], whose relaxation frequency, in the pure phase, is about 17 GHz at room temperature (see figure 1). Water is the principal component of most aqueous solutions of interest, and has a large orientational electric polarization. The large dielectric increment of water ($\Delta\varepsilon = 75.9$ for pure water at 20 °C) [2] is partly due to the large dipole of 1.84 debye for a water molecule and partly caused by the high Kirkwood correlation factor, associated with the extended network of hydrogen-bonded clusters of water molecules [15–17]. Although the presence of the charged polymers alters both the dielectric increment and the relaxation frequency, the main characteristics do not differ from those of the bulk water dispersion, the difference being confined to a shift in the relaxation time and a generally moderate decrease in the dielectric increment. These changes could be important to control the biological function of a large variety of biopolymers but they seem to have little influence on the dynamical properties associated with polymers in aqueous solution. The water within a few molecular diameters of a polyion (so-called bound water) [2] has appreciably different properties than bulk water. The relaxation of this hydration layer depends on the organization

of that layer, ranging from kHz for ice-like structures to hundreds of MHz for less hindered structural organization.

In the intermediate-frequency range, usually between 1 and 100 MHz, another relaxation occurs, whose origin has long been controversial. Three ideas have been suggested for this intermediate frequency relaxation.

(1) The van der Touw and Mandel model [18, 19] envisions the polyion as a sequence of subunits and counterion fluctuation along each of them imparts an induced dipole moment along the polymer chain whose relaxation causes the observed dielectric dispersion. This proposed mechanism is independent of the polyion molecular weight and we shall use this essential idea to describe the low-frequency relaxation of polyelectrolyte solutions in section 4.3.
(2) The theory developed independently by Dukhin and Fixman strongly suggested that the intermediate frequency relaxation is caused by motion of *free* counterions. This prompted later models of Mandel to focus on the exchange between bound and free counterions, in a direction perpendicular to the polyelectrolyte chain [20, 21]. Ito *et al* [22] expanded on this idea to predict the observed power-law behaviour of relaxation time [23, 24] and dielectric increment [22, 25, 26] as a function of polyelectrolyte concentration, from the simple assumption that the intermediate frequency relaxation results from the fluctuation of free counterions on the scale of the correlation length that is characteristic of semi-dilute polyelectrolyte solutions. This model is described in section 4.2.
(3) For polyions that have a dipolar component perpendicular to the chain contour, Mashimo *et al* [27, 28] attributed the molecular mechanism responsible for the intermediate relaxation region to electrical dipole fluctuations caused by Brownian motion of the polymer chain. The influence of the local structure of the chain has been recently investigated in the case of poly(lysine), poly(α-glutamate) and poly(γ-glutamate) aqueous solutions [29–31].

Generally, a dependence of the dielectric parameters on the polymer concentration should be expected. This dependence is particularly intriguing, because of the delicate interplay between local chain conformation and effective polyion charge, each of which can depend on the concentration, flexibility and contour length of the polyelectrolyte, and its interactions with small ions (counterions and added salt).

In the remainder of this section, we briefly summarize the main aspects of current understanding of dielectric response. These features are illustrated with dielectric spectra of two representative polyelectrolyte solutions.

1.2. Complex dielectric constant: phenomenology

From an experimental point of view, the dielectric response $\epsilon^*(\omega)$ of a given system to an external oscillatory electric field of angular frequency ω is given by the linear relationship

$$\langle \vec{J} \rangle = \mathrm{i}\omega\epsilon_0\epsilon^*(\omega)\vec{E} \tag{4}$$

between the volume-averaged current density

$$\langle \vec{J} \rangle = \frac{1}{V}\int_V \vec{J}(\vec{r})\,\mathrm{d}V \tag{5}$$

and the electric field

$$\vec{E} = -\frac{1}{V}\int_V \nabla\Psi(\vec{r})\,\mathrm{d}V, \tag{6}$$

where $\Psi(\vec{r})$ is the electric potential at position $\vec{r}$, V is a sufficiently large system volume and ϵ_0 is the dielectric constant of free space. Regardless of the origin of the relaxation process, the complex dielectric constant $\epsilon^*(\omega)$ is related to the time correlation function $\phi(t)$ of the macroscopic dipole moment of the volume V in time t in the absence of an applied electric field, by the one-side Fourier transform

$$\frac{\epsilon^*(\omega)-\epsilon_\infty}{\epsilon_s-\epsilon_\infty} = 1 - \mathrm{i}\omega\int_0^\infty \phi(t)\exp(-\mathrm{i}\omega t)\,\mathrm{d}t, \tag{7}$$

where ϵ_s and ϵ_∞ are the limiting low- and high-frequency permittivities, respectively.

If $\phi(t)$ is characterized by a single exponential decay with a time constant τ, equation (7) yields the well-known Debye relaxation function [1]

$$\frac{\epsilon^*(\omega)-\epsilon_\infty}{\epsilon_s-\epsilon_\infty} = \frac{1}{1+\mathrm{i}\omega\tau}. \tag{8}$$

For many materials, the dipole correlation function $\phi(t)$ exhibits a non-exponential shape, often represented by the Kohlrausch–Williams–Watts equation [32, 33]

$$\phi(t) = \exp\left(-\frac{t}{\tau}\right)^\gamma \tag{9}$$

with $0 < \gamma < 1$, the distribution parameter. This relaxation function leads to a dielectric relaxation function analogous to the Cole–Davidson function which has been extensively used to describe the frequency domain dielectric relaxation data. A detailed comparison of the two non-exponential relaxation functions, that behave similarly in a time scale or frequency scale over several decades, has been carried out by Lindsey and Patterson [34] and by Alvarez *et al* [35].

An extensively used empirical modification of equation (8) reads

$$\frac{\epsilon^*(\omega)-\epsilon_\infty}{\epsilon_s-\epsilon_\infty} = \frac{1}{[1+(\mathrm{i}\omega\tau)^\beta]^\alpha}, \tag{10}$$

resulting in the Cole–Cole relaxation function ($\alpha = 1$, $0 < \beta < 1$) [36], the Cole–Davidson relaxation function ($\beta = 1$, $0 < \alpha < 1$) [37, 38] or the Havriliak–Negami relaxation function ($0 < \alpha < 1$, $0 < \beta < 1$) [39]. Equation (10), which contains two further parameters (α and β) in comparison with the simple Debye relaxation (equation (8)), is often found to give a good description of the asymmetric loss spectra observed in polymer solutions over the whole frequency interval where the relaxation falls.

Alternately, for a non-single-exponential decay correlation function, equation (8) may be rewritten, by introducing a distribution of relaxation times $g(\tau)$, as

$$\frac{\epsilon^*(\omega)-\epsilon_\infty}{\epsilon_s-\epsilon_\infty} = \int \frac{g(\tau)\,\mathrm{d}\tau}{1+\mathrm{i}\omega\tau}. \tag{11}$$

Explicit functional forms for the distribution function $g(\tau)$ leading to Cole–Cole, Cole–Davidson and Havriliak–Negami relaxation functions have been discussed by Böttcher and Bordewijk [40]. In cases where two or more relaxation processes overlap, two or more distinct relaxation functions may be employed.

For a polymer chain with degree of polymerization N, the response function $\phi(t)$ is written as a normalized correlation function

$$\phi(t) = \frac{\sum_{i=1}^{N} \langle \mu_i(t)\mu_i(0)\rangle}{\sum_{i=1}^{N} \langle \mu_i(0)\mu_i(0)\rangle}, \tag{12}$$

where $\mu_i(t)$ is the dipole moment of the ith repeat unit at time t. Equation (12) can be decomposed [33, 41, 42] into contributions of the dipole moment components perpendicular $\mu^{\perp}$ and parallel $\mu^{\parallel}$ to the chain contour

$$\phi(t) = \left\langle \sum_{i=1}^{N} \mu_i^{\parallel}(t) \sum_{i=1}^{N} \mu_i^{\parallel}(0) + \sum_{i=1}^{N} \mu_i^{\perp}(t) \sum_{i=1}^{N} \mu_i^{\perp}(0) \right\rangle. \tag{13}$$

The laws governing the time decay of $\phi(t)$ are directly related to the structural and kinetic properties of the sample and characterize the macroscopic electrical properties of the system investigated. The first term of equation (13) reflects the overall rotation of the polymer molecule and, if the polymer is completely random, the dipole correlation is given by

$$\phi^{\parallel}(t) = (\mu^{\parallel})^2 \langle R_i(t) R_i(0)\rangle, \tag{14}$$

where $R_i(t)$ is the end-to-end vector of the ith segment which causes the low-frequency dispersion process. The second term of equation (13) represents the autocorrelation function of the perpendicular dipole moment component. This term is sensitive to segmental motion of the polymer chain and can contribute to the intermediate frequency relaxation. The presence of a dipole component perpendicular to the polyion backbone, according to equation (13), has been used in the analysis of the intermediate relaxation process occurring in poly(amino acid) aqueous solutions [29, 43]. According to Mashimo [27, 28], it is noteworthy that orientation of the ith perpendicular component requires a conformational change of neighbouring repeat units that could be the origin of the subunits in the Mandel model [7].

1.3. Dielectric loss and electrical modulus

The complex dielectric constant $\epsilon^*(\omega)$ is usually written as

$$\varepsilon^*(\omega) = \varepsilon'(\omega) - \mathrm{i}\frac{\sigma(\omega)}{\varepsilon_0 \omega}, \tag{15}$$

where ω is the angular frequency (2π times the frequency ν in Hz), $\varepsilon'(\omega)$ is the real part of the complex dielectric constant, $\sigma(\omega)$ is the total conductivity and ε_0 is the permittivity of vacuum. The measured dielectric loss $\sigma(\omega)/(\varepsilon_0\omega)$ is made up of two components. One is due to the dielectric process $\varepsilon''(\omega)$ and the other is due to the dc electrical conductivity σ_0, which is the low-frequency limit of $\sigma(\omega)$. The general expression of equation (15) is then

$$\varepsilon^*(\omega) = \varepsilon'(\omega) - \mathrm{i}\left[\varepsilon''(\omega) + \frac{\sigma_0}{\varepsilon_0\omega}\right]. \tag{16}$$

The dc conductivity loss $\sigma_0/(\varepsilon_0\omega)$ increases with decreasing frequency and often obscures $\varepsilon''(\omega)$ due to the dielectric processes of interest at the lowest frequencies. As stated above, this circumstance makes low-frequency dielectric measurements difficult and the interpretation of the data doubtful, if a rigorous and powerful data analysis is not performed.

In some cases, to overcome this difficulty, an alternative approach to calculate the dielectric parameters from the electrical modulus can be adopted. The complex electrical modulus (or complex inverse permittivity) $M^*(\omega)$ can be used to represent the frequency-dependent data:

$$M^*(\omega) = \frac{1}{\varepsilon^*(\omega)} = M'(\omega) + \mathrm{i}M''(\omega). \tag{17}$$

The real and imaginary parts of the electrical modulus are

$$M'(\omega) = \frac{\varepsilon'(\omega)}{[\varepsilon'(\omega)]^2 + [\varepsilon''(\omega) + \sigma_0/\varepsilon_0\omega]^2}, \tag{18}$$

$$M''(\omega) = \frac{\varepsilon''(\omega) + \sigma_0/\varepsilon_0\omega}{[\varepsilon'(\omega)]^2 + [\varepsilon''(\omega) + \sigma_0/\varepsilon_0\omega]^2}. \tag{19}$$

This formalism is particularly advantageous when the system exhibits a frequency-dependent conductivity, as it usually occurs in polymer solutions, since the monotonically increasing function describing the total loss transforms into a curve exhibiting a peak corresponding to a particular frequency that varies proportionally with the low-frequency conductivity σ_0 [44]. This peak is shifted towards higher frequencies, simplifying the deconvolution of the dielectric dispersion from the contributions due to the dc conductivity.

The fundamental effects in polyion solutions influencing the overall dielectric response in different frequency ranges [45] are classical dipole orientation, polarization of the counterion atmosphere, polarization associated with the internal degrees of freedom of the polymer chain and dielectric relaxation caused by fast chemical relaxation processes. They provide information not only about structural characteristics (dipole moments, rotational diffusion coefficients) but also on properties of the counterion atmosphere (ion mobility and density, 'effective' dielectric constant) as well as on kinetic parameters (chemical relaxation time, rate constants) and on the influence of an electric field on the chemical equilibria in the solution.

1.4. Dielectric spectra of polyelectrolyte solutions: two examples

In this section, we summarize the results of dielectric measurements on two typical polyelectrolytes, a double-stranded helical molecule with a large persistence length (DNA) and a synthetic polyion considered as a model system for a flexible chain polyelectrolyte (sulfonated polystyrene). In both examples, different relaxation regions, covering the frequency range from 1 kHz to some tens of GHz, have been observed.

The presence of negatively charged phosphate groups in the nucleotide chain makes DNA a highly charged linear polyelectrolyte. A variety of molecular mechanisms, on different length scales, simultaneously contribute to the dielectric response of DNA. A typical dielectric spectrum in the range from 1 kHz to 70 GHz, obtained by merging dielectric spectra measured by Takashima *et al* [46] and by the Mandel group [19], is shown in figure 2 (upper panel). Three dielectric dispersions are evident, a low-frequency dispersion located between 1 and 100 kHz, an intermediate-frequency dispersion between 1 and 500 MHz and a high-frequency dispersion above 1 GHz.

The low-frequency (10–100 kHz) relaxation is not caused by the rotation of the permanent dipole moment of the entire DNA molecule, since the dielectric increment of this low-frequency relaxation increases with added salt [47, 48] but, instead must be assigned to the condensed counterion polarization along the whole polyion. The intermediate-frequency relaxation is attributed to fluctuations of counterions along some well-defined sections of the chain ('subunits' in the Mandel model and the semi-dilute correlation length in the Ito model).

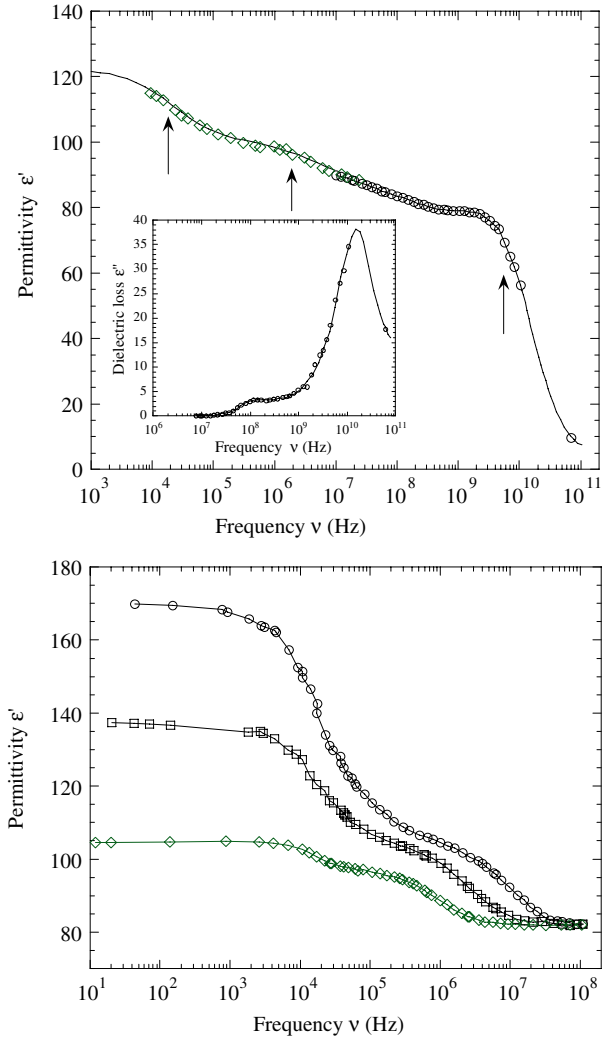

Figure 2. Top: permittivity of 1% DNA aqueous solutions over the frequency range from 10 kHz to 100 GHz. The data are obtained by merging dielectric spectra in the low-frequency range from Mandel and co-workers [19] at 0.17% and spectra in the high-frequency range from Takashima *et al* [46] at 1%. The Mandel data have been shifted vertically to match the different DNA concentrations. The inset shows the dielectric loss related to the intermediate and high-frequency relaxations. Bottom: permittivity of NaPSS ($M_w = 177\,000$) at three different concentrations: (○) 1.380 g l^{-1}, (□) 0.450 g l^{-1} and (◇) 0.090 g l^{-1}. The drawn curve is the fitted double Cole–Cole relaxation function (data from Mandel [49]).

The high-frequency relaxation is due to the orientational polarization of water molecules (see figure 1).

The second example, shown in figure 2 (lower panel), shows the dielectric response of three aqueous solutions of sodium poly(styrene sulfonate) (NaPSS), recently investigated by Mandel [49] up to a frequency of 100 MHz, below the high-frequency relaxation of water. For sufficiently high molecular weights, two separate dispersion regions are observed, whose main features can be summarized as follows. The low-frequency dispersion can be quite

large, with a specific dielectric increment and relaxation time that are molecular weight dependent. Conversely, the parameters of the generally smaller, higher-frequency dispersion are independent of molecular weight. All parameters depend on polyelectrolyte concentration and also depend on the type and concentration of the added salt. Both observed dispersions are attributed to counterion fluctuations on two different typical distances associated with the polymer conformation.

Despite considerable differences in the conformations of the polymers in these two examples, the dielectric spectra are quite similar. This is not surprising, since both polymers are essentially immobile on these time scales and hence, the relaxations near 10 kHz and near 1 MHz are believed to be due to motion of sodium counterions.

2. Experimental methods

2.1. Circuitry and impedance analysers

We will discuss in some detail only frequency domain dielectric spectroscopy (FDDS), which is usually employed for the measurement of the complex permittivity of samples characterized by high permittivity and conductivity, such as aqueous electrolytes. In the frequency domain, the complex permittivity of the sample can be measured, at various discrete frequencies, with high accuracy, to determine the dielectric spectrum in a specific frequency range. However, time domain spectrometers have been recently improved in accuracy and in their performance with aqueous, highly conductive samples [4, 50]. An excellent review on the use of time domain dielectric spectroscopy in investigating emulsions and colloidal systems has been recently published [51].

The sample is usually contained in an appropriate sample holder, the 'dielectric cell', even though for special purposes dielectric probes have been designed that can be immersed into the liquid or simply held near its surface [52, 53]. Since, different parasitic effects dominate in different frequency ranges, it is not possible to devise a single dielectric cell that can be effectively employed in the whole frequency range of interest in the study of polyelectrolyte solutions (from a few kHz up to a few GHz). While at the low-frequency end of the spectrum (below 1 MHz) the plane parallel capacitor geometry is usually adopted [54–58], at higher frequencies, in order to reduce inductive effects, open-ended coaxial probes are preferable [59, 60].

The possibility of using simple and accurate bridge techniques for the measurement makes FDDS very attractive. Although the upper frequency limit of most commercial bridges was in the past limited to a few hundred MHz [57, 61, 62], commercial impedance analysers based on the current–voltage method ('auto-balancing' bridges) are now available [63, 64] that allow precise, rapid and automated measurements, over a wide impedance and frequency range (up to a few GHz).

From the measured impedance, the dielectric parameters that characterize the sample have to be extracted and separated from the contributions of cell geometric capacitance, connecting cables, etc. At the low-frequency end of the spectrum, where the geometry is that of a 'plane capacitor', the usual procedure is to model the cell as seen by the meter using an equivalent circuit, with elements that take into account the different contributions to the total measured impedance [56, 57, 61, 62, 65]. At higher frequencies, where the approximation of 'concentrated elements' is no longer valid, different methods are used [59, 66, 67].

2.1.1. Low-frequency range (Hz to MHz). In the low-frequency range, the measuring cell can be described by means of the equivalent elements circuit as shown in figure 3 [57], however

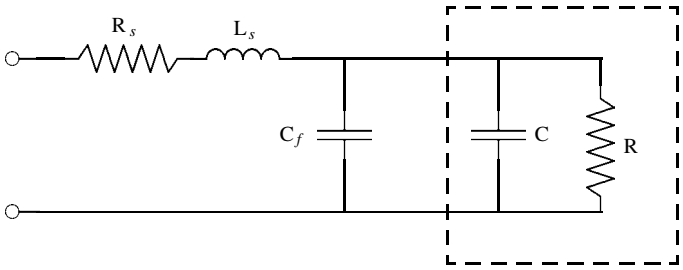

Figure 3. The equivalent circuit of the measuring cell for low-frequency measurements, as seen by the meter. R_s, L_s and C_f represent parasitic effects (connecting cable impedance, fringe effects, etc); C_0 is the empty cell capacitance, $C = \varepsilon' C_0$ is the sample capacitance and $R = \varepsilon_0/(\sigma C_0)$ is the sample resistance.

other equivalent circuits have been proposed [56, 61, 62, 65, 68]. Usually, the series resistance R_s is small compared with the total impedance and can be neglected. The contribution to the series inductance L_s due to connecting cables is also negligible at low frequencies, but the contribution of the cell itself, usually, cannot be neglected, since the parallel plate geometry shows a high self-inductance. For a parallel plate capacitor, with circular electrodes separated by a distance d, and where the current is fed from the centre (radial current), the self-inductance is estimated from the expression [69]

$$L = \frac{\mu_0}{4\pi}\frac{d}{2} \tag{20}$$

(μ_0 is the magnetic permeability of free space $\mu_0 = 4\pi \times 10^{-7}\,\mathrm{H\,m^{-1}}$). With this geometry, considering electrodes 2 cm in diameter and 1 mm apart, filled with an aqueous solution ($\varepsilon' \simeq 80$), at frequencies of about 1 GHz the magnitude of the inductive impedance ($|Z_L| = \omega L$) becomes comparable to the capacitive one ($|Z_C| = 1/\omega C$). However, with the simple plane parallel geometry also at frequencies of a few tens of MHz, the effect of the parasitic inductance can produce unacceptable distortion in the measured dielectric spectra. The use of a cylindrical grounded shield, whose axis is identical with that of the cell ('nearly coaxial' geometry [58]), effectively reduces both the stray-field effects (fringe effects, represented by the capacitance C_f), and the self-inductance [58, 70]. In figure 3, C and R, representing the capacitance and the resistance of the sample, can be expressed in terms of the sample permittivity ε' and conductivity σ as

$$C = C_0\varepsilon' \qquad \text{and} \qquad 1/R = C_0\sigma/\varepsilon_0, \tag{21}$$

where C_0 is the so-called 'cell constant', i.e. the capacitance of the empty cell, that also includes all the effects due to field inhomogeneities.

The different parameters that characterize the equivalent circuit can be obtained by means of proper calibration procedures, using different standard liquids of known permittivity and conductivity [57].

A very simple and reliable calibration procedure consists of measuring the cell impedance in three different configurations: shorted cell electrodes (Z_s), the empty cell (Z_e), and the cell filled with a standard sample (Z_l) of known dielectric permittivity ε'_l and conductivity σ_l. In these three configurations, the measured impedances reduce to

$$Z_s = R_s + \mathrm{i}\omega L_s, \tag{22}$$

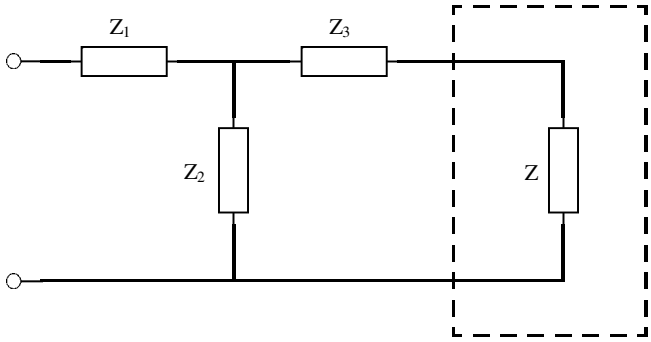

Figure 4. In the higher-frequency range, the equivalent circuit of the measuring cell can be modelled as a T network; Z represents the sample impedance.

$$Z_e = R_s + \mathrm{i}\left[\omega L_s - \frac{1}{\omega(C_f + C_0)}\right], \tag{23}$$

$$Z_l = R_s + \mathrm{i}\left\{\omega L_s - \frac{1}{\omega[C_f + C_0(1+\varepsilon_l')] - \mathrm{i}\sigma_l C_0/\varepsilon_0}\right\}, \tag{24}$$

respectively. By combining these expressions, the whole set of parameters is easily obtained.

Then, from the measured impedance $Z = |Z|\cos\phi + \mathrm{i}|Z|\sin\phi$, and using equations (21)–(24) (now written for the unknown sample) the total conductivity σ and the dielectric permittivity ε' are calculated as

$$\sigma = \frac{\varepsilon_0}{C_0}\frac{|Z|\cos\phi - R_s}{(|Z|\cos\phi - R_s)^2 + (|Z|\sin\phi - \omega L_s)^2}, \tag{25}$$

$$\varepsilon' = \frac{1}{C_0}\left\{\frac{|Z|\cos\phi - R_s}{\omega[(|Z|\cos\phi - R_s)^2 + (|Z|\sin\phi - \omega L_s)^2]} - C_f\right\}. \tag{26}$$

2.1.2. High-frequency range (MHz to GHz). At higher frequencies (above several MHz), self-inductance effects become of paramount importance. The simple plane parallel geometry is no longer effective and the impedance of even the shortest connecting cables is no longer negligible. At these frequencies, the dielectric cell usually consists of a short section of a coaxial line, terminated by a standard connector (APC7, for example) directly connected to the meter [59–61].

The measuring cell can hence be described by means of an equivalent 'T network' as shown in figure 4 [59]. The impedances Z_1, Z_2 and Z_3 can be expressed in terms of the input and output impedances of a classical four terminal network as

$$Z_1 = Z_{o1} - \sqrt{Z_{o2}(Z_{o1} - Z_{s1})}, \quad Z_2 = Z_{o2} - \sqrt{Z_{o2}(Z_{o1} - Z_{s1})}, \quad Z_3 = \sqrt{Z_{o2}(Z_{o1} - Z_{s1})},$$

where Z_{o1} and Z_{s1} are the input impedances when the output is open and shorted, respectively, and Z_{o2} and Z_{s2} are the corresponding output impedances.

The impedance as seen by the meter, Z_m, can then be written as

$$Z_m = Z_1 + \frac{Z_3(Z_2 + Z)}{Z_3 + Z_2 + Z} \tag{27}$$

or, equivalently

$$Z_m = \frac{Z + (Z_{s1}Z_{o2}/Z_{o1})}{(Z_{o2}/Z_{o1}) + (Z/Z_{o1})}, \tag{28}$$

where Z is the sample impedance (see figure 4). From this expression, the sample impedance Z can be obtained as a bilinear function of the measured impedance Z_m, in the form

$$Z = \frac{\alpha Z_m - \beta}{1 - \gamma Z_m}, \tag{29}$$

where $\alpha = Z_{o2}/Z_{o1}$, $\beta = Z_{s1}Z_{o2}/Z_{o1}$ and $\gamma = 1/Z_{o1}$.

In practice, the complex parameters α, β and γ, that describe the electrical behaviour of the measuring cell, taking into account the cell geometry and the parasitic effects, can be determined by means of a calibration procedure: measuring the impedance when the cell is empty, shorted and filled with a sample of known permittivity and conductivity or, alternatively, using three different standard liquids of known dielectric parameters.

In fact, using the result that the composition of two bilinear transformations in the complex plane is still a bilinear transformation, the complex permittivity ε^* of the unknown sample can be determined straightforwardly from the measured complex impedance, Z^*, solving the bilinear equation [67]

$$\frac{(\varepsilon^* - \varepsilon_1^*)(\varepsilon_2^* - \varepsilon_3^*)}{(\varepsilon^* - \varepsilon_2^*)(\varepsilon_1^* - \varepsilon_3^*)} = \frac{(Z^* - Z_1^*)(Z_2^* - Z_3^*)}{(Z^* - Z_2^*)(Z_1^* - Z_3^*)}, \tag{30}$$

where $Z_j^* = |Z_j|\mathrm{e}^{-\mathrm{i}\phi_j}$, with $j = 1, 2, 3$, are the complex impedances measured when the coaxial line cell is filled with three different liquids of known complex dielectric permittivity ε_j^*, used as calibration standards.

This calibration procedure can have the advantage of using standards whose dielectric parameters are 'in the vicinity' of the unknown sample, making the calibration more precise. Moreover, the measurement of the cell's true 'short' and/or 'open' impedance is often difficult, because of fringe effects and residual admittances.

For example, in the case of polyelectrolyte aqueous solutions, three NaCl solutions of appropriate molarities, with conductivities extending over the range of the samples investigated, can be used as reference liquids. For each electrolyte solution, the complex dielectric permittivity as a function of the electric field frequency ω is written as

$$\varepsilon^*(\omega) = \varepsilon_\infty + \frac{\varepsilon_w - \varepsilon_\infty}{1 + \mathrm{i}\omega\tau_{\mathrm{H_2O}}} + \frac{\sigma_0}{\mathrm{i}\omega\varepsilon_0} \tag{31}$$

where ε_∞ is the high-frequency limiting permittivity, ε_w is the dielectric constant of water at frequencies below the water relaxation ($\omega \ll 1/\tau_{\mathrm{H_2O}}$), $\tau_{\mathrm{H_2O}}$ is the relaxation time of water, σ_0 is the dc conductivity (the low-frequency limit of the total conductivity) and ε_0 is the permittivity of vacuum. The parameters ε_w, ε_∞, $\tau_{\mathrm{H_2O}}$ and σ_0 can be calculated for different molarities and temperatures [71] (see appendix).

Repeated measurements on reference liquids of known conductivity and dielectric constant allow to estimate the overall accuracy of the procedure. In the typical range of conductivities of high charge density polyelectrolyte solutions, from diluted to concentrated regimes, the overall accuracy has been estimated to be within 2% on ε' and within 5% on ε'' [25], for sufficiently high frequencies that the dc conductivity can be subtracted. The uncertainties increase markedly as frequency is lowered, owing to conductivity and electrode polarization effects dominating the measurements.

2.2. Analysis of dielectric and conductometric spectra

The dielectric parameters characterizing the dispersion, i.e., the dielectric increment $\Delta\varepsilon$, the characteristic relaxation time of the process τ and the 'spread parameters' β and α (see equation (32), for example), which characterize the distribution of relaxation times around τ, are usually determined by a non-linear least-squares minimization on the basis of a well-defined relaxation function such as, for example, the Havriliak–Negami equation (equation (10)) [1, 39, 72]. If different relaxation phenomena are observed in the frequency range investigated, the dielectric spectrum is analysed on the basis of a sum of different relaxation functions. As an example, the dielectric response of a typical polyelectrolyte solution, in the frequency range from a few kHz to a few GHz, can be described as a sum of three relaxations:

$$\varepsilon^*(\omega) = \varepsilon'(\omega) - \mathrm{i}\varepsilon''(\omega) = \frac{\Delta\varepsilon_1}{[1 + (\mathrm{i}\omega\tau_1)^{\beta_1}]^{\alpha_1}} + \frac{\Delta\varepsilon_2}{[1 + (\mathrm{i}\omega\tau_2)^{\beta_2}]^{\alpha_2}} + \frac{\varepsilon_w - \varepsilon_\infty}{1 + (\mathrm{i}\omega\tau_{\mathrm{H_2O}})^{\alpha}} + \varepsilon_\infty. \tag{32}$$

The first term (with a characteristic relaxation frequency of the order of some tens of kHz) is usually attributed to the polarization of condensed counterions along the whole polymer chain, while the second is attributed to the free counterion relaxation along some well-defined characteristic length. Finally, the third term is approximately Debye-like (the spreading parameter α is near unity, see appendix and figure 8), and takes into account the contribution of the dielectric response of water. In aqueous solutions, at frequencies above a few tens of MHz, the orientational relaxation of the water molecules cannot be neglected, considering that the maximum loss in the dielectric dispersion of pure water occurs at a frequency of about 17 GHz, at room temperature. This dispersion produces an increase of the total conductivity at frequencies above a few tens of MHz (see, for example, figure 5). This increase represents the low-frequency tail of the relaxation process associated with the polarization of water molecules, which in equation (32) is modelled by the Debye function (with $\alpha = 1$) with a dielectric increment $\Delta\varepsilon_{\mathrm{H_2O}} = \varepsilon_w - \varepsilon_\infty$, and relaxation time $\tau_{\mathrm{H_2O}}$.

In the example of figure 5, the huge increase in the low-frequency wing of the dielectric constant is due to the superposition of two effects: a further dispersion mechanism (the 'low-frequency dispersion' described by the first term in equation (32)) and the electrode polarization effect, which will be discussed in section 2.3.

In general, it is difficult to resolve different dielectric dispersions when their relaxation times are within a factor of ten from each other. Conversely, the assessment of the different contributions is even more complicated when, from outside the frequency range experimentally accessible, only the 'tails' of different well-separated dispersions partially overlap.

A satisfactory estimate of the parameters of the dispersion can often be obtained by means of a non-linear least-squares fitting procedure based on the Levenberg–Marquardt algorithm for complex functions [2]. The method allows the simultaneous fit of the real part (the permittivity $\varepsilon'(\omega)$) and the imaginary part (the dielectric loss $\varepsilon''(\omega)$) of the complex dielectric constant $\varepsilon^*(\omega)$ or, alternatively, the simultaneous fit of $\varepsilon'(\omega)$ and the total loss $\sigma(\omega)/\varepsilon_0\omega$ [25, 73]. In this way, due to the constraints imposed on the fitting procedure by the dispersion relation between the real and imaginary parts of the complex permittivity, a reliable estimate of the parameters of the dispersion is obtained, even in the cases where, considering a separate fit, the dispersion could not have been conveniently resolved.

However, since the whole shape of the dielectric loss spectrum $\varepsilon''(\omega)$ depends strongly on the low-frequency conductivity $\sigma_0 \equiv \lim_{\omega\to 0}\sigma(\omega)$ to be subtracted from the total loss $\sigma(\omega)/\varepsilon_0\omega$, an accurate analysis of the fitting procedure is required. A preliminary simultaneous

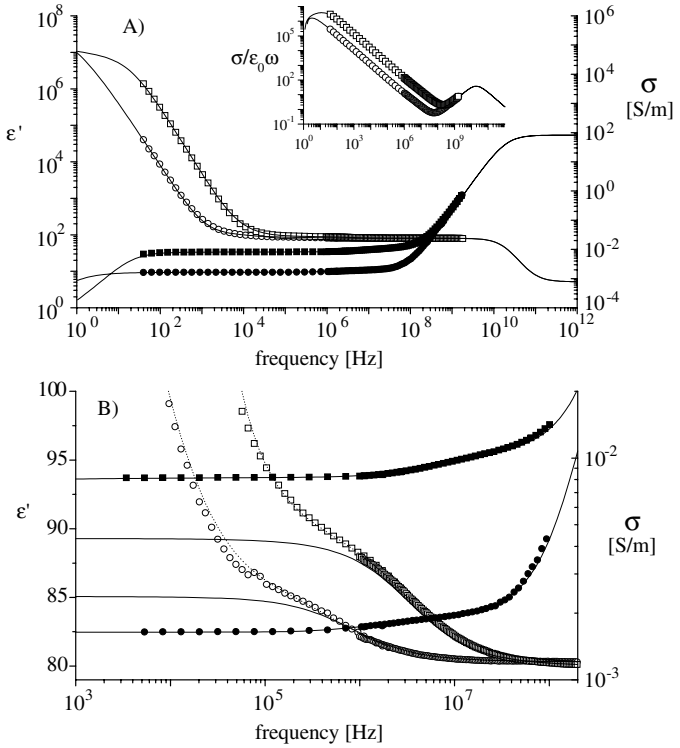

Figure 5. (A) The measured permittivity ε' (open symbols) and total conductivity σ (filled symbols) of aqueous solutions of a typical high charge density polyelectrolyte, NaPAMS (sodium salt of poly[2-acrylamido-2-methylpropanesulfonate]), as a function of frequency, at two different polymer concentrations: (□) 40.5 mg g^{-1}; (○) 1.14 mg g^{-1}; temperature $T = 20\,^{\circ}$C. The inset shows the corresponding curve for $\sigma/\varepsilon_0\omega$, the 'total' dielectric loss $\varepsilon''(\omega)+(\sigma_0/\varepsilon_0\omega)$, also including the effect of the ohmic (dc) conductivity σ_0. The steep increase observed in the conductivity at the higher frequencies is due to the dielectric polarization of water. At frequencies $\lesssim$100 kHz, the electrode polarization effect becomes appreciable, as it produces a steep increase in the values of measured ε' and, at the lowest frequencies, a decrease in the conductivity σ. The solid lines represent the values calculated on the basis of equations (32) and (37) and take into account the electrode polarization effect. The dielectric parameters were estimated by the simultaneous fitting of the real and imaginary parts of $\varepsilon^*(\omega)$, using the procedure described in the text, based on the Levenberg–Marquardt method for complex functions. (B) An enlarged view of a portion of (A), showing the 'intermediate frequency' relaxation due to the polyelectrolyte; in this case the 'low frequency' relaxation is completely masked by the huge polarization effect, and also the 'high-frequency' relaxation would be difficult to resolve properly without a careful analysis of the data. In (B), the solid lines are calculated from equation (32), after subtraction of the polarization effect; for comparison, dotted lines are the calculated ones but without this subtraction (same as in (A)).

fit of $\varepsilon'(\omega)$ and the total loss $\sigma(\omega)/\varepsilon_0\omega$, with $\Delta\varepsilon$, τ, β, ε_∞ and σ_0 as free parameters and $\alpha = 1$, gives a first rough estimate. From the value of σ_0 thus obtained, the dielectric loss is calculated as $\varepsilon''(\omega) = [\sigma(\omega) - \sigma_0]/\varepsilon_0\omega$ and the simultaneous fit is repeated on $\varepsilon'(\omega)$ and $\varepsilon''(\omega)$. The whole procedure should be iterated until the set of parameters, $\Delta\varepsilon$, τ, β, ε_∞ and σ_0, converges and a good fit is achieved. This procedure gives a set of parameters that describes the observed behaviour with satisfactory accuracy, even in the case where the dc electrical conductivity of the samples investigated is relatively high [25, 73].

2.3. Electrode polarization

In the measurement of the dielectric properties of conductive solutions, the well-known 'electrode polarization' effect, mainly due to the spatial charge that accumulates near the electrodes, represents a serious obstacle. The presence of this electrical 'double layer' modifies the field distribution within the sample. This effect, to a first approximation, can be described as a 'surface impedance', mainly capacitive, in series with the sample impedance [74–77]. This electrode impedance makes it difficult, and often even impossible, to resolve the dielectric dispersions at lower frequencies. For this reason, it is worth to discuss briefly here the different strategies that can be implemented to cope with this problem.

The many different approaches that have been proposed to correct for the electrode polarization effects [2] can be roughly grouped in two categories. The first category includes the methods aimed to eliminate or reduce the impact of the effect. The second group includes methods for correcting the measured dielectric spectra, taking into account the presence of surface impedance.

Within the first group, special measurement techniques have been devised such as the four-electrode method [3, 78, 79], and the electromagnetic induction method [80, 81]. The four-electrode method is based on the observation that the double layer builds up at the surface of the two current electrodes, but not at the two inner high-impedance voltage-sensing electrodes, since in this case the input current is virtually zero. In the electromagnetic induction method, two toroidal coils are employed as the voltage and current 'electrodes' and the complex permittivity is deduced from the measured coupling of the two coils.

An effective and far simpler method to reduce electrode polarization is to use of electrodes with a large surface area, thus reducing the effect of the double layer capacitance (in series with the bulk capacitance). To this end, the effective surface of electrodes can be hugely increased (by a factor of 100–1000 times) with respect to the geometrical surface by using microporous electrodes. For example, by depositing a layer of 'platinum black' (electro-deposited colloidal platinum), the effective surface area of the electrodes can be substantially increased [82–84].

Other methods are based on the use of a cell with variable electrode spacing [2, 58, 85–87]. Since the sample impedance depends on the electrode spacing, while the polarization impedance does not, it is possible to separate the contribution of the electrode polarization from a set of measurements at different spacings. In practice, the capacitance at each frequency is linear in reciprocal electrode spacing [87] and extrapolated to $1/d = 0$ to obtain the sample capacitance. This method was used by Mandel and co-workers to determine the low-frequency data in figure 2, for example.

In substitution methods [82, 88–90], the electrode polarization impedance is eliminated by means of calibration with simple electrolytes of known conductivity. However, these methods rely on the assumption that the effects on the electrodes of the electrolyte used for calibration are the same as those of the ions in the sample.

Although many methods have been proposed, an entirely satisfactory solution to the problem of reducing the electrode polarization is not known. This is in part due to our incomplete understanding of the underlying mechanisms of this complex phenomenology. Electrode polarization depends on the ionic conductivity, through the concentration and the nature of the ionic species in the solution, the temperature, the physico-chemical state of the electrodes, the 'history' of their contact with the test liquid and, in general, the physico-chemical parameters that characterize the bulk phase. This last feature, in particular, would make it preferable that the method used to correct the measured dielectric spectra takes into account the presence of exactly that sample which is actually under test. In fact, since electrode polarization depends on the nature and chemical composition of the sample (and of the electrodes) and both

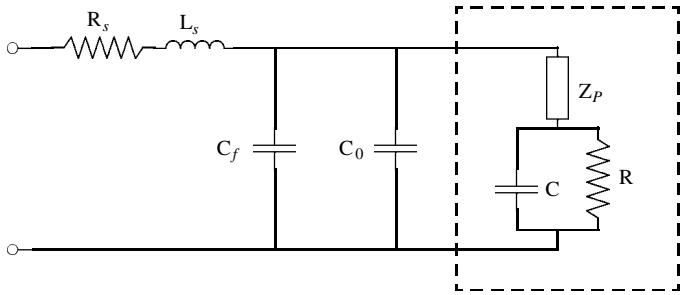

Figure 6. The equivalent circuit of the measuring cell, as in figure 3, but with the CPA element representing the polarization effect in series with the sample impedance.

of them may change over time (in particular for biological samples, or when chemical reactions take place during the measurements), it would be highly desirable to have a method where the correction is not performed comparing the measured dielectric spectrum with 'something else' but on the basis of the measured spectrum alone. This result can be obtained modelling the effect of the polarization as a characteristic electrode impedance with a proper frequency dependence in series with the sample admittance (figure 6) and fitting the full expression to the raw experimental data.

This scheme has been extensively employed, usually assuming, for the frequency dependence of the real and imaginary parts of the electrode impedance, power laws with fractional exponents [50, 91, 92]. However, the electrode surface impedance can be more effectively described by using the expression [50, 93–95]

$$Z_p = K^{-1}(\mathrm{i}\omega)^{-\alpha}, \tag{33}$$

usually indicated as a constant phase angle (CPA) element. This expression has obvious advantages, compared to simple power laws applied separately to correct the real and imaginary parts of the measured dielectric constant (and/or conductivity), because the dispersion relationships are fulfilled. As a consequence, the exponents of the asymptotic power laws for the real and imaginary parts are not independent (this decreases the number of independent parameters that have to be obtained from the fitting procedure). In the above expression, K is a constant and the exponent $0 \leqslant \alpha \leqslant 1$ depends on the characteristics of the electrode surface. For a perfectly smooth and homogeneous surface (as in the case of a liquid mercury electrode), the behaviour is purely capacitive and $\alpha = 1$, while for a 'porous' electrode [94] α should be equal to $1/2$. The presence of a relationship between the exponent α and the fractal dimension of the electrode surface has been postulated by various authors [93, 94, 96–98]. For fractal electrodes with a known surface fractal dimension, D_f, built up by photo-etching, Nyikos and Pajkossy [97, 98] have obtained the relationship

$$\alpha = \frac{1}{D_f - 1} \tag{34}$$

and have derived, for the constant K in equation (33), the expression

$$K = f_g \sigma_0^{1-\alpha}, \tag{35}$$

where f_g is a purely geometric factor and σ_0 is the bulk conductivity of the electrolyte solution. These simple models have been criticized from both theoretical [96, 99] and numerical [100] points of view. Furthermore, there are several recent experimental studies showing that CPA behaviour is not correlated with the 'electrode geometry' (meaning roughness on a

microscopic scale) but rather with the combined effect of adsorption [101, 102] and electrode inhomogeneities on the 'nanoscopic' scale [103] (as probed by Atomic Force Microscopy). However, although the physical origin of CPA behaviour appears to be different from what was postulated by the earliest studies on this subject, there is a general consensus on using this equivalent circuit to model the electrode impedance.

Within this scheme, in the presence of an electrode polarization contribution, the sample admittance $Y_s(\omega) = 1/R + i\omega C$ has to be replaced with the sum

$$Z_m(\omega) = Z_p(\omega) + \frac{1}{Y_s(\omega)} \tag{36}$$

and, as a result, the measured equivalent complex dielectric constant $\varepsilon^*_{eq}(\omega)$ is written as

$$\varepsilon^*_{eq}(\omega) = \frac{\varepsilon'(\omega) - i[\varepsilon''(\omega) + (\sigma_0/\varepsilon_0\omega)]}{1 + (C_0/K)(i\omega)^{1-\alpha}\{\varepsilon'(\omega) - i[\varepsilon''(\omega) + (\sigma_0/\varepsilon_0\omega)]\}}, \tag{37}$$

where $\varepsilon'(\omega)$ and $\varepsilon''(\omega)$ are the real and imaginary parts, respectively, of the sample permittivity (given, for example, by equation (32)) and σ_0 is the low-frequency limit of the conductivity.

In figure 5 the typical dielectric spectrum of a high charge density polyelectrolyte is shown, measured over a wide frequency range. The steep increase observed in conductivity at frequencies above 10^8 Hz (and the corresponding maximum in ε'' at $\approx$17 GHz) is due to the dielectric polarization of water (see figure 1).

At these values of the ohmic conductivity (typical of polyelectrolyte aqueous solutions in the semi-dilute concentration regime), the electrode polarization effect becomes appreciable at frequencies $\lesssim$0.1–1 MHz. Polarization produces a steep increase in the values of the measured ε' and, at lower frequencies, a marked decrease in the conductivity σ. The solid lines in figure 5(B) represent the calculated values on the basis of equations (32) and (37), taking into account the electrode polarization effect. In figure 5(B), showing an enlarged portion of the spectra, the solid lines are calculated from equation (32) after subtraction of the polarization effect. From the figure, it is clear that correction for this effect is absolutely necessary in order to obtain meaningful parameters of the dielectric dispersion due to the polyelectrolyte solution.

3. Background theory for polyelectrolyte solutions

Before delving into the analysis of dielectric spectra on polyelectrolyte solutions, it is important to present some background on two crucial inter-related issues: counterion condensation and the chain conformation. In this section, we summarize the main results of the simplest views on these subjects, as the more sophisticated theories have been reviewed previously [5–11]. For our purposes here, the simple views suffice, with the caveat that the physics of polyelectrolyte solutions remains an unsolved problem.

3.1. Counterion condensation

Electrical transport properties of aqueous polyelectrolyte solutions, owing to the strong electrostatic interactions between counterions in the solution and charged groups on the polyion chain, greatly differ from those of neutral macromolecular solutions and those of simple electrolytes [5, 11, 13, 14, 104–112]. Current models for polyelectrolyte solutions are generally based on counterion condensation, first introduced by Imai and Onishi [107], Oosawa [5, 110] and later by Manning [13, 111, 112].

The basic idea is that when the charge density on a linear polyelectrolyte chain exceeds a critical value, this excess charge must in part be neutralized by the counterions in the solution. 'Free' counterions will then 'condense' in the vicinity of the chain to such an extent that the Coulomb repulsion energy of two adjacent charged groups on the chain becomes smaller than the thermal energy kT. The extent of this condensation should depend, in principle, on the fine interplay between electrostatic interactions and the change in entropy due to the spatial confinement of the counterions 'near' the polyion. Although, there is a general consensus on this qualitative picture that is supported by a huge amount of experimental evidence [11], the details of the physical mechanism from which counterion condensation ensues are still matters of debate [113–115], and different approaches to the 'condensation' problem have been elaborated [113, 116–120]. Indeed, particularly for multivalent counterions, the positions of the condensed ions are thought to be highly correlated along the chain, forming a one-dimensional 'Wigner crystal' [121]. Although the main results of Manning's counterion condensation model [13, 111, 112, 122] are fairly well-satisfied by experimental data, the theory appears insufficient to describe satisfactorily the observed behaviour at finite concentration (see, for example, [26, 43, 114, 123–126]), and other theories have been proposed [127].

The local conformation of the polyelectrolyte chain is the result of a delicate balance between chain-solvent interactions and electrostatic repulsion, so that the 'charged line' model is a rather crude approximation. Particularly in semi-dilute solution, effects associated with the polymer chain conformation become relevant, and their influence on the overall electrical properties of the polyelectrolyte solutions must be properly considered [119, 128–131].

Manning developed a model for the electrical conductivity of polyelectrolyte solutions [122, 132–134] that has been the main reference model in the field, mainly by virtue of its simplicity. Often the Manning model is preferred over other approaches to develop theories for the colligative and electrical transport properties of linear polyelectrolyte solutions.

Consider a polyelectrolyte solution, made up of polyion chains, each with a degree of polymerization N (suppose, for simplicity, that each monomer bears only one charged group of valence z_p), contour length L, monomer size b and $N|z_p|/|z_1|$ counterions of valence z_1.

According to the Manning condensation model [13, 111, 112, 122], the system is characterized by a charge-density parameter, defined as the ratio of the Bjerrum length (equation (2)) and the charge spacing along the chain,

$$\frac{l_B}{b} = \frac{e^2}{\varepsilon_w kTb}, \tag{38}$$

where ε_w is the dielectric constant of water, kT is the thermal energy and $b = L/N$ is the average spacing between charged groups on the polyion chain. If the charge spacing is too small, the electric field becomes so strong that the system can lower its free energy by condensing some of the counterions on the polyion chain. The Manning criterion for counterion condensation

$$\frac{l_B}{b} > \frac{1}{|z_p z_1|} \tag{39}$$

states that when the charge density along the chain ($|z_p|/b$) exceeds the largest allowed value, i.e., when charge spacing becomes $<|z_1|l_B$, counterions condense to decrease the effective charge density to the maximum allowed value. The Manning model predicts that a fraction $1 - f = 1 - b/(l_B|z_1 z_p|)$ of the counterions will condense on the polyion chain to reduce its effective charge density. Only fraction $f = b/(l_B|z_1 z_p|)$ of the counterions are free in solution, leaving each polyion bearing an effective charge $Q_p = z_p eNf$.

3.2. The de Gennes scaling model

In 1976, de Gennes *et al* [135] proposed a simple scaling model for the conformation of polyelectrolytes. Since that time, the model has been verified by small-angle neutron scattering [136] and has been successfully extended to model polyelectrolyte dynamics [130] (viscosity and diffusion). On very small scales (of the order of a few monomers), there is insufficient charge repulsion to modify the chain conformation. On such small scales, the chain adopts a conformation consistent with the thermodynamic interaction between uncharged monomers and solvent. In most cases, the solvent is water and the uncharged polymer would not dissolve in water—this case is referred to as 'poor solvent'. In such a case, the polyelectrolyte is locally collapsed, shielding as many monomers as possible from the unfavourable interaction with water. The size ξ_e of these collapsed electrostatic blobs of g_e monomers is given by a balance between the electrostatic energy inside the blob and the interfacial free energy of the electrostatic blob surface [130, 137].

$$\frac{(efg_e)^2}{\varepsilon\xi_e} \approx \left(\frac{\tau\xi_e}{b}\right)^2 kT \qquad \text{poor solvent.} \tag{40}$$

Here, e is the elementary charge, f is the fraction of monomers bearing an effective charge, ε is the dielectric constant, $\tau \equiv (\theta - T)/\theta$ is the reduced temperature (θ being the temperature at which the net interaction between uncharged polymer and water is zero) and b is the monomer size. The chain is collapsed inside the electrostatic blob, with $\xi_e \approx b(g_e/\tau)^{1/3}$. Combining with equation (40) determines the electrostatic blob size in poor solvent.

$$\xi_e \approx \frac{b^{4/3}}{f^{2/3}l_B^{1/3}} \qquad \text{and} \qquad g_e \approx \frac{\tau b}{f^2 l_B} \qquad \text{poor solvent.} \tag{41}$$

Here, l_B is the Bjerrum length (equation (2); $l_B = 7.12\,\text{Å}$ in water at 20 °C), where the Coulomb interaction energy between two elementary charges is equal to the thermal energy. It is instructive to input typical parameter values for polyelectrolytes in poor solvent: $b \cong 7\,\text{Å}$ and $f \cong 0.2$, making $\xi_e \cong 20\,\text{Å}$. A typical reduced temperature is $\tau \cong 0.5$, making $g_e \cong 10$.

It is also possible to have a polyelectrolyte in a good solvent that would swell the uncharged chain and hence swell the electrostatic blob. In this case, the electrostatic blob size is determined by a balance between the electrostatic energy inside the blob and the thermal energy kT [130, 135].

$$\frac{(efg_e)^2}{\varepsilon\xi_e} \approx kT \qquad \text{good solvent.} \tag{42}$$

The chain is swollen inside the electrostatic blob in good solvent, with $\xi_e \approx bg_e^{3/5}$. Combining with equation (42) determines the electrostatic blob size in good solvent.

$$\xi_e \approx \frac{b^{10/7}}{f^{6/7}l_B^{3/7}} \qquad \text{and} \qquad g_e \approx \left(\frac{b}{f^2 l_B}\right)^{5/7} \qquad \text{good solvent.} \tag{43}$$

Inputting the same parameter values as used above ($b \cong 7\,\text{Å}$ and $f \cong 0.2$) suggests that $\xi_e \cong 30\,\text{Å}$ and $g_e \cong 10$. Therefore, the electrostatic blobs in a good solvent contain roughly the same number of monomers as in poor solvent, but their size is appreciably larger, with more solvent inside the electrostatic blob. For both good solvent and poor solvent conditions, the net charge of the electrostatic blob is roughly $2e$ ($fg_e \cong 2$). These charges most likely reside at the outer surface of the electrostatic blob.

Both theory [131, 138, 139] and simulation [138, 140] suggest that the local conformation of polyelectrolytes in poor solvent can be far more interesting than the simple electrostatic

blob picture. Regions of strong local collapse, with diameter D_b, are separated by strongly stretched strings of length l_s in some instances in poor solvent (the pearl necklace). For most of our purposes, these details are not essential, and we use the simple de Gennes electrostatic blob picture in our description of polyelectrolyte solutions here. This effectively maps the beads and strings (or whatever other local conformations [139, 140]) onto a cylinder of diameter ξ_e.

In a dilute solution in any polar solvent, a flexible polyelectrolyte with no added salt adopts a highly extended (directed random walk) conformation with length L determined by the strong electrostatic repulsion between the N/g_e electrostatic blobs in the chain.

$$L \approx \xi_e \frac{N}{g_e} \qquad \text{dilute solution.} \tag{44}$$

The distance between chains R_{cm} in dilute solutions is proportional to the $-1/3$ power of concentration c (the number density of monomers).

$$R_{cm} \approx \left(\frac{N}{c}\right)^{1/3} \qquad \text{dilute solution.} \tag{45}$$

As concentration c is increased, the polyelectrolyte size begins to decrease in the vicinity of the overlap concentration.

$$c^* \approx \frac{N}{L^3} \approx \frac{(g_e/\xi_e)^3}{N^2}. \tag{46}$$

In semi-dilute solutions (above the overlap concentration), the polyelectrolytes maintain their highly extended conformation up to the correlation length ξ, while on larger scales the chains are random walks [135]. The correlation length ξ is independent of chain length and decreases as the concentration is increased.

$$\xi \approx L\left(\frac{c}{c^*}\right)^{-1/2} \approx \left(\frac{g_e}{\xi_e c}\right)^{1/2} \qquad \text{semi-dilute solution.} \tag{47}$$

Owing to the strong repulsion between correlation volumes, semi-dilute polyelectrolyte solutions with no added salt are divided into correlation volumes that are essentially identical, as depicted in figure 7. Each correlation volume has $g = c\xi^3$ monomers with $fc\xi^3$ counterions.

$$g \approx g_e \frac{\xi}{\xi_e} \qquad \text{semi-dilute solution.} \tag{48}$$

In semi-dilute solutions, the polyelectrolyte chain is a random walk of correlation volumes, with end-to-end distance R.

$$R \approx \xi\left(\frac{N}{g}\right)^{1/2} \approx \left(\frac{\xi_e}{g_e c}\right)^{1/4} N^{1/2} \qquad \text{semi-dilute solution.} \tag{49}$$

4. Dielectric response of polyelectrolyte solutions

4.1. High-frequency relaxation of water

The high-frequency relaxation, at a frequency of order 10 GHz, is due to the orientation polarization of water and is associated with the correlated organization of individual water molecules in extended hydrogen-bonded clusters [15–17], under the influence of the external electric field [141]. This picture is substantiated by considering that the self-diffusion coefficient of water D and the dielectric relaxation time of water τ_{H_2O} have the same activation

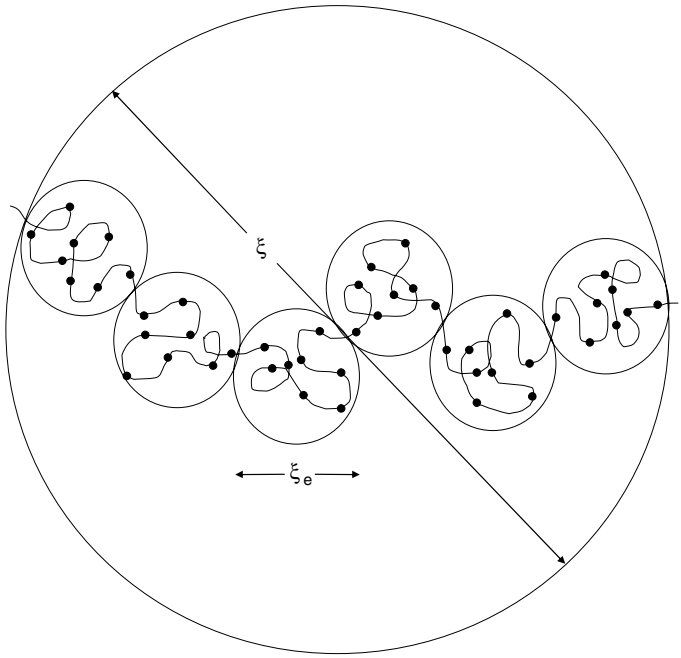

Figure 7. The correlation volume in semi-dilute solution (the large circle) is a directed random walk of electrostatic blobs (small circles) with effectively charged monomers (●). Each effectively charged monomer has a free counterion (not shown) somewhere in the correlation volume.

enthalpy (18.8 kJ mole^{-1}) corresponding to the breaking of one hydrogen bond, and viscosity divided by absolute temperature η/T has an activation enthalpy of 18.1 kJ mole^{-1}, indicating that the same molecular mechanism is responsible for all three processes.

For liquid water, the dependence of the dielectric relaxation time τ_{H_2O} on temperature is well accounted for by the Debye equation [1]

$$\tau_{H_2O} = 4\pi a^3 \frac{\eta}{kT}, \tag{50}$$

where a is the radius of a water molecule and kT is the thermal energy. Using the temperature dependences of the dielectric relaxation time and the viscosity of water between 0 and 100 °C, the Debye equation determines that $a = 1.44$ Å for water, independent of temperature. With or without polyelectrolyte present, the high-frequency relaxation process can be adequately represented by a single time constant τ_{H_2O}, as the deviations from a single Debye-type relaxation function are extremely small. The temperature dependence of the dielectric parameters ε_w, ε_∞, τ and α for the orientational polarization of water are shown in figure 8.

The presence of charged polymers in water partially modifies the dielectric characteristics of the orientational water molecule relaxation due to a change of the dielectric constant of water surrounding the charged sites on the polymer chain. Consequently, the water molecules close to the polyion will be differently organized from those of the bulk water and will respond to the electric field with a different relaxation time. However, theoretical calculations and numerical simulations of the dielectric constant of this bound water have shown that the effect is confined to a region around the charge that does not extend beyond 2–3 Å and that rapidly the permittivity of the water reaches the value of pure water. Although the high-frequency relaxation of water in aqueous polyion solutions is different from that in pure water and the

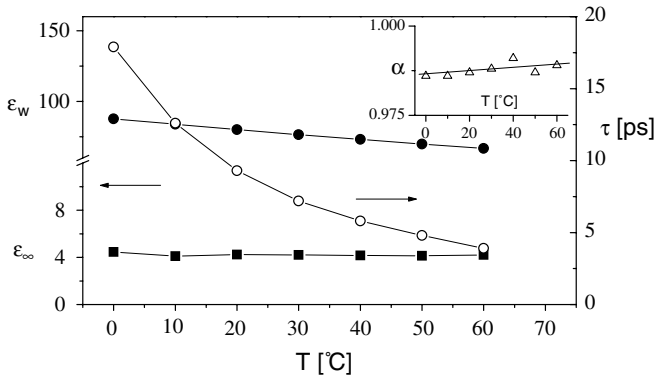

Figure 8. Effect of temperature on the parameters describing the dielectric relaxation of water (see appendix): (●) ε_w, (■) ε_∞ and (○) τ. The relaxation-time spread parameter α (inset, △) is almost constant and, in the analysis of relaxation spectra of polyelectrolyte solutions, is generally assumed to be 1 (Debye relaxation). Values shown in this plot are those reported by Hasted [1], based on an analysis of the collected available data using a Cole–Cole relaxation function.

dielectric parameters such as relaxation time, relaxation strength and Cole–Cole parameter depend on polymer concentration [142, 143], the influence is very small on the relaxation of the polyion and its counterions, which occur at much lower frequencies.

The strong dipole–charge interaction between water molecules and charged groups on the polymer chains makes the bound water irrotational with a partially ice-like structure [144]. The hindered orientation of the bound water should give rise to a dielectric dispersion occurring at frequencies around 100–500 MHz [2], intermediate between that of pure water (17 GHz) and that of ice (1–5 kHz). The presence of polyelectrolytes can impart a considerable increase of the free ion concentration in water, influencing, due to the strong localized electric field, the water molecule organization. A typical change of the dielectric parameters of the orientational water relaxation induced by NaCl salt at different concentrations is shown in figure 9. However, at the polyion concentrations of primary interest, the increase of ion concentration due to dissociation and ionization of the charged groups of the polymer is relatively small, making for very small changes in the high-frequency dielectric relaxation of aqueous polyelectrolyte solutions. The dielectric strength associated with the bound water is generally small compared with the intermediate frequency relaxation of free counterions, making an accurate determination of the relaxation of bound water difficult for polyelectrolyte solutions. This is unfortunate because the bound water is believed to play an important role in the biological functions of many biopolymers, such as DNA and proteins [2]. These aspects are outside the scope of this review and will not be discussed further here. However, the dielectric relaxations of proteins occur at sufficiently low frequency that the relaxation of bound water can be isolated [2]. The activation enthalpy of bound water (29 kJ mol^{-1}) [2] is considerably larger than that for bulk water.

4.2. Intermediate frequency relaxation of free counterions

The relaxation at intermediate frequencies has been studied for many years. Early models assumed that this relaxation was the result of polarization of bound counterions along the polyelectrolyte. However, the 1974 work of Dukhin [145, 146] and the 1980 work of Fixman [147–150] clearly establish the role of the *free* counterions in the theoretical interpretation of

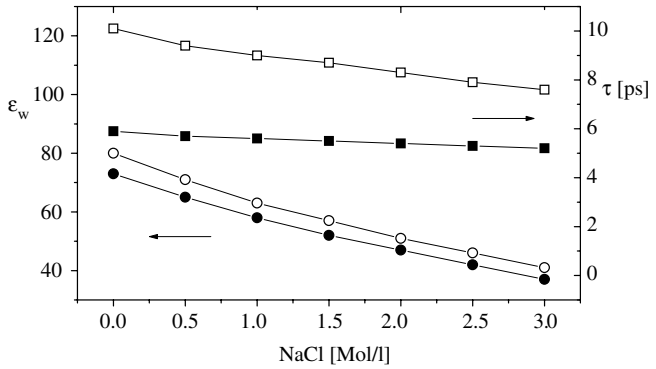

Figure 9. Changes induced by the added NaCl electrolyte on the dielectric parameters of the orientational water relaxation ((○, ●) ε_w; (□, ■) τ), at two different temperatures ((○, □) 20 °C; (●, ■) 40 °C) that are a typical example of the effects of dissolved ions on the dielectric behaviour of water.

intermediate relaxation. Polarization of free counterions in the so-called double-layer have dominated the models appearing since that time.

Experimentally, Ito and co-workers [151] have used frequency-domain electric birefringence spectroscopy to show that low-frequency relaxation involves polarization along the polyelectrolyte chain, while intermediate relaxation corresponds to polarization perpendicular to the chain backbone. More recent birefringence experiments [23, 24] on sulfonated polystyrene have shown that the intermediate relaxation time increases as the chain is neutralized with NaOH for small values of the extent of neutralization, $\alpha < 0.6$. At low extents of neutralization, the Na^+ counterions are predominantly free, so this increase in relaxation time strongly suggests that the intermediate relaxation involves *free* counterions. Further increase in the extent of neutralization essentially adds counterions that are condensed on the chain backbone and the relaxation time becomes independent of α [23] for $\alpha > 0.5$. Furthermore, as the counterion is varied, the intermediate relaxation frequency is observed to be proportional to the mobility of free counterions in water [24]. These birefringence measurements comprise the most direct experimental proof that the intermediate relaxation involves polarization of free counterions.

4.2.1. The free-counterion polarization model of Ito. Based on their experimental observation of polarization perpendicular to the chain backbone [151], Ito and co-workers proposed a simple model for intermediate frequency relaxation [22]. In dilute solution, the free counterions can polarize by free diffusion in three-dimensional space to a scale of the order of the distance between chains (equation (45)).

$$\tau_{ion} \approx \frac{R_{cm}^2}{6D} \approx \frac{N^{2/3}}{6Dc^{2/3}} \qquad \text{dilute solution.} \tag{51}$$

Here, D is the diffusion coefficient of the counterion in solution. The polarizability of each free counterion, α_{ion}, is determined by the square of their charge e^2 (for univalent counterions) and the polarization distance R_{cm}.

$$\alpha_{ion} \approx \frac{e^2 R_{cm}^2}{kT} \approx \frac{e^2 N^{2/3}}{kTc^{2/3}} \qquad \text{dilute solution.} \tag{52}$$

The dielectric increment of the intermediate relaxation $\Delta\varepsilon$ in dilute solution is simply the product of the number density of free counterions fc and their polarizability.

$$\Delta\varepsilon \approx fc\alpha_{ion} \approx \frac{fe^2N^{2/3}c^{1/3}}{kT} \approx fl_B\varepsilon N^{2/3}c^{1/3} \qquad \text{dilute solution.} \tag{53}$$

In semi-dilute solution, the free counterions can polarize by simple diffusion within the correlation volume. The time scale for such a relaxation τ_{ion} is the time required for counterions to diffuse a distance of the order of the correlation length in three-dimensional space (equation (47)).

$$\tau_{ion} \approx \frac{\xi^2}{6D} \approx \frac{g_e}{6D\xi_e c} \qquad \text{semi-dilute solution.} \tag{54}$$

The free counterion polarizability is determined by their charge e and polarization distance ξ.

$$\alpha_{ion} \approx \frac{e^2\xi^2}{kT} \approx \frac{e^2 g_e}{kT\xi_e c} \qquad \text{semi-dilute solution.} \tag{55}$$

The dielectric increment of the intermediate relaxation is once again the product of the number density of free counterions and their polarizability.

$$\Delta\varepsilon \approx fc\alpha_{ion} \approx \frac{fe^2 g_e}{kT\xi_e} \approx fl_B\varepsilon\frac{g_e}{\xi_e} \qquad \text{semi-dilute solution.} \tag{56}$$

The fraction of monomers bearing an effective charge f can be obtained by either combining equations (51) and (53) in dilute solution or equations (54) and (56) in semi-dilute solution.

$$f \approx \frac{\Delta\varepsilon}{6D\tau_{ion}l_B\varepsilon c}. \tag{57}$$

4.2.2. Comparison with data. One of the most extensively studied polyelectrolytes is NaPSS, and the data for the intermediate relaxation time of NaPSS with no added salt at various concentrations and molecular weights are shown in figure 10, where two concentration regimes are evident. At low concentrations, $\tau_{ion} \sim c^{-2/3}$ as expected by equation (51). At high concentrations, $\tau_{ion} \sim c^{-1}$ as expected by equation (54). The data for the intermediate relaxation dielectric increment $\Delta\varepsilon$ of NaPSS at various concentrations and molecular weights are shown in figure 11. These data also exhibit the expected crossover in the vicinity of c^*. Low concentrations have $\Delta\varepsilon \sim c^{1/3}$ as expected by equation (53), while high concentrations have $\Delta\varepsilon$ nearly independent of concentration, as expected by equation (56).

The crossover concentrations between the two regimes for both dielectric increment and relaxation time are plotted as a function of the degree of polymerization in figure 12. Also plotted in figure 12 are the overlap concentrations estimated from the concentration at which the specific viscosity is unity [152] and the concentration where the wavevector of the peak in small-angle x-ray scattering crosses from $c^{1/3}$ to $c^{1/2}$ (another measure of the overlap concentration) [153]. Figure 12 shows that the crossover concentrations for dielectric increment and relaxation time, while not identical, are quite comparable with the overlap concentration c^* estimated by other methods and are roughly proportional to N^{-2}, as predicted by equation (46).

4.3. Low-frequency relaxation of bound counterions

Low-frequency relaxation has been studied less extensively than intermediate frequency relaxation. The principal reason for this is that conductivity and electrode polarization issues make the low-frequency relaxation challenging to resolve. The polyelectrolyte chain is expected

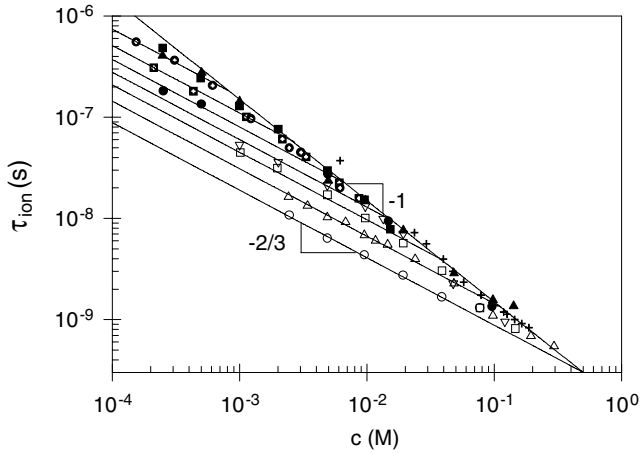

Figure 10. Concentration dependence of the intermediate relaxation time of NaPSS solutions in water, for different degrees of polymerization N. Data are those of Ito [22] at 20 °C ($N = 87$ (○); $N = 170$ (△); $N = 350$ (□); $N = 500$ (▽); $N = 1000$ (●); $N = 2000$ (▲); $N = 3800$ (■)), Mandel [49] at 21 °C ($N = 860$ crossed squares; $N = 1700$ crossed circles) and Bordi [25] at 20 °C ($N = 5800$ (+)).

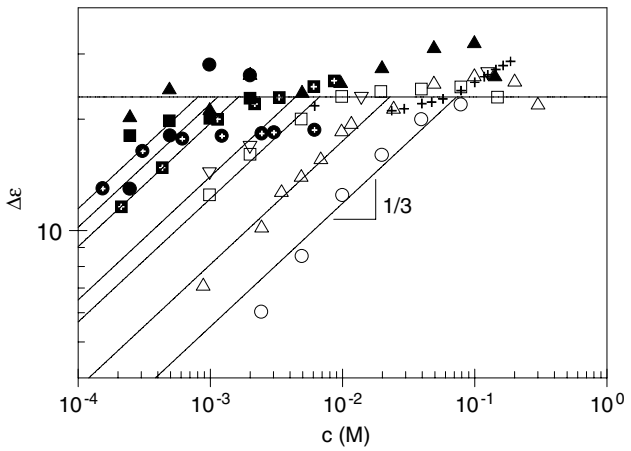

Figure 11. Concentration dependence of the intermediate relaxation dielectric increment of NaPSS solutions in water. Symbols are the same as in figure 10.

to be stationary on the time scale of low-frequency dielectric relaxation. Since intermediate frequency relaxation involves polarization of the free counterions and occurs on much shorter time scales, low-frequency dielectric relaxation most likely originates from polarization of the condensed counterions along an essentially stationary polyelectrolyte chain.

There are $(1 - f)N$ condensed counterions on each chain. Fluctuations of condensed counterions [108, 109] should create charges of order $\pm e[(1 - f)N]^{1/2}$ occurring over a distance comparable with the end-to-end distance of the chain R. The induced dipole moment from thermal fluctuations is

$$\alpha \approx \frac{e^2(1 - f)NR^2}{kT} \approx l_B \varepsilon (1 - f)NR^2. \tag{58}$$

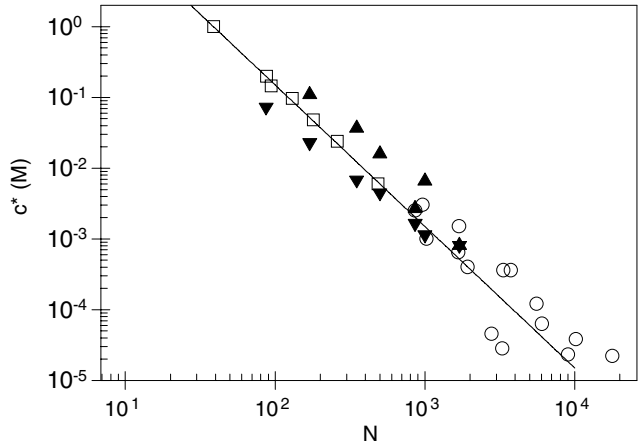

Figure 12. Dependence of the overlap concentration on the degree of polymerization for NaPSS. Data are estimates from (□) SAXS [153], (○) viscosity [152], (▲) the intermediate relaxation time data of figure 10 and (▼) the dielectric increment data of figure 11. The line has the slope of −2 as expected by equation (46).

Assuming that each chain polarizes independently, the dielectric increment for low-frequency dielectric relaxation should be the product of the induced dipole moment of a single chain α and the number density of chains (c/N).

$$\Delta\varepsilon \approx l_B\varepsilon(1-f)cR^2. \tag{59}$$

In dilute solutions, the relevant chain size is given by equation (44), while in semi-dilute solutions the chain size is given by equation (49). Polarization of condensed counterions should give a dielectric increment

$$\Delta\varepsilon \approx l_B\varepsilon(1-f)c\left(\frac{\xi_e N}{g_e}\right)^2 \approx l_B\varepsilon(1-f)\frac{g_e}{\xi_e}\frac{c}{c^*} \qquad \text{dilute solution,} \tag{60}$$

$$\Delta\varepsilon \approx l_B\varepsilon(1-f)N\left(\frac{\xi_e c}{g_e}\right)^{1/2} \approx l_B\varepsilon(1-f)\frac{g_e}{\xi_e}\left(\frac{c}{c^*}\right)^{1/2} \qquad \text{semi-dilute solution.} \tag{61}$$

The dielectric increment of low-frequency relaxation has been reported by Mandel [49] for two molecular weights of NaPSS and the data are shown in figure 13. The data do not extend over a wide concentration range, and that range spans c^* for both samples. Hence, it is not surprising that the data exhibit an apparent exponent for the concentration dependence of $\Delta\varepsilon$ that is between the $1/2$ expected in semi-dilute solution and the unity expected in dilute solution. However, the apparent dependence of $\Delta\varepsilon$ on molecular weight is considerably stronger than expected. The large corrections involved in isolating the low-frequency relaxation may be responsible for this and more data are clearly needed.

Figure 14 compares the low-frequency dielectric relaxation times (open symbols) with the intermediate-frequency relaxation times (filled symbols), the polyelectrolyte chain relaxation times (solid lines) and the correlation volume relaxation times (broken line). Polyelectrolyte chain relaxation times were estimated as R_g^2/D using the diffusion coefficients reported by Oostwal *et al* [154] on the same two NaPSS samples ($M = 177\,000$ has $D = 6.2\times10^{-12}$ m^2 s^{-1} and $M = 354\,000$ has $D = 3.0\times10^{-12}$ m^2 s^{-1}, independent of concentration in the semi-dilute

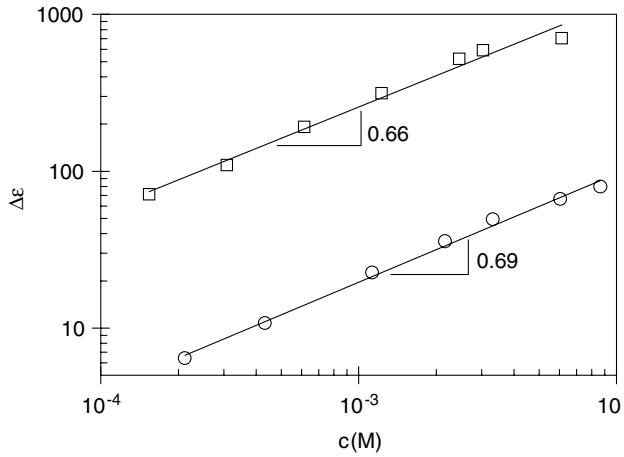

Figure 13. Dielectric increment from the low-frequency dielectric relaxation of NaPSS [49]. $M = 177\,000$ (◯) and $354\,000$ (□). The lines have slopes between unity expected below c^* and $1/2$ expected above c^*.

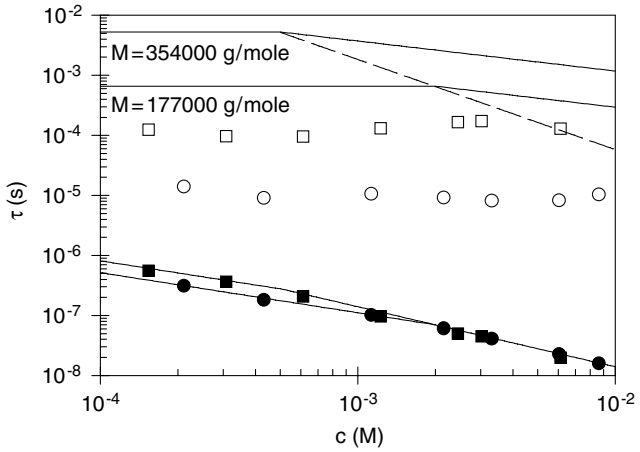

Figure 14. Relaxation times from the low-frequency (τ_{bound}, ○, □) and intermediate frequency (τ_{ion}, ●, ■) dielectric relaxations of NaPSS ($M = 177\,000$ are circles and $M = 354\,000$ are squares) [49]. The lines associated with the intermediate frequency data have slopes of $-2/3$ below c^* and -1 above c^* (see figure 10). The solid lines at the top of the figure are the longest polyelectrolyte relaxation times estimated from diffusion data on the same polymers [154]. The broken line is the estimated relaxation time of a correlation volume. Since the low-frequency relaxation times are much shorter than any of the chain relaxation times, the low-frequency relaxation is attributed to fluctuations of condensed counterions along an immobile chain.

unentangled regime) and the SANS measures of concentration (c in moles of monomer per litre) and molecular weight (M in g mole^{-1}) dependences of the radius of gyration (R_g in nm) of NaPSS in semi-dilute solution [155–157].

$$R_g = 0.032 M^{1/2} c^{-1/4}. \tag{62}$$

It is clear from figure 14 that low-frequency dielectric relaxation has a relaxation time that is shorter than any of the polyelectrolyte chain relaxation times. Low-frequency dielectric

relaxation time is also insensitive to concentration, even at the highest concentrations studied, in contrast to the polyelectrolyte chain relaxation times in semi-dilute solution, which show concentration dependences [129, 130, 152, 158]. The relaxation time of the low-frequency relaxation is determined by the friction coefficient ζ for condensed counterions moving along the stationary polyion backbone.

$$\tau_{bound} \approx \frac{\zeta L^2}{6kT}. \tag{63}$$

Using the chain contour length (equation (44)) we determine the relaxation time for polarization of condensed counterions.

$$\tau_{bound} \approx \frac{\zeta}{6kT}\left(\frac{\xi_e N}{g_e}\right)^2 \tag{64}$$

We can estimate the friction coefficient by combining equations (59) and (63).

$$\zeta \approx 6(1-f) l_B \varepsilon c k T \frac{\tau_{bound}}{\Delta\varepsilon}. \tag{65}$$

Using the data of Mandel [49], we estimate that $\zeta = 3 \times 10^{-7}$ g s^{-1} for condensed sodium counterions on NaPSS in dilute solution at 21 °C, roughly a factor of 100 larger than the ζ for free sodium counterions [159] (kT/D). If correct, this estimate casts some doubts on the idea that condensed counterions organize a Wigner crystal [121].

5. Electrical conductivity of polyelectrolyte solutions

Here, we review the electrical conductivity of aqueous polyelectrolyte solutions, in light of the counterion condensation theory of section 3.1, using the scaling concepts of section 3.2 in the description of the polyion chain in different concentration regimes. Electrical conductivity as a useful probe of the transport of charged objects in an external electric field has a long history. Recently, significant advances have been made, since our understanding of the coupling between chain conformation and counterion condensation has improved.

We focus on the ac electrical conductivity σ_0, measured at low frequencies, for solutions of charged particles uniformly dispersed in a continuous (conducting or non-conducting) medium. In practice, this conductivity measurement does not require the sophisticated equipment needed for dielectric measurements at high frequencies, discussed in section 2. Inexpensive conductivity meters are available that employ multiple low frequencies (to ensure that the low frequency limit is realized), temperature compensation and a four-electrode design (see section 2.3) to provide conductivity measurements on aqueous solutions with high precision.

Quite generally, the conductivity σ_0 is due to the sum of contributions of all the charge carriers in the system, given by

$$\sigma_0 = \sum_i (|z_i|e) n_i \mu_i, \tag{66}$$

where z_i is the valence, n_i the number concentration and μ_i the mobility (ratio of velocity and electric field) of the different carriers. This equation can be rewritten in more convenient units as

$$\sigma_0 = \sum_i z_i c_i \lambda_i, \tag{67}$$

where c_i is the concentration (in mol cm^{-3}) and λ_i is the specific conductance (in Ω^{-1} cm^2 mol^{-1}) of each carrier in the solution.

For polyelectrolyte solutions without salt and in the presence of counterion condensation, equation (67) reads

$$\sigma = z_1 c_1 \lambda_1 + z_p c_p \lambda_p, \tag{68}$$

where the subscripts 1 and p refer to counterions and polyions, respectively. For univalent counterions ($z_1 = 1$), the following relationships hold, $c_1 = fc$, $z_p = fN$ and $c_p = c/N$, where c is the molar concentration of monomer (moles of monomer cm^{-3}) and N is the number of monomers per chain. Equation (68) becomes

$$\sigma = fc(\lambda_1 + \lambda_p) \tag{69}$$

for univalent counterions. Equation (69) depends on three parameters: the fraction f of free counterions and the equivalent conductances, λ_1 and λ_p, of counterions and polyions, respectively. The various models for polyelectrolyte conductivity make different predictions for these three parameters.

5.1. Manning model for dilute solutions

Following the Manning derivation [122, 132–134], the conductivity of a dilute salt-free polyelectrolyte solution must be modified to account for the reduced mobility of the counterions in the presence of the polyion

$$\sigma = fc\frac{D_1}{D_1^0}(\lambda_1^0 + \lambda_p), \tag{70}$$

where D_1^0 and D_1 are the diffusion coefficients of counterions in the limit of infinite dilution and in the presence of polyions, respectively, and λ_1^0 is the equivalent conductance of free counterions without the polyions present. Manning [13] derived for D_1/D_1^0 the value 0.866.

The equivalent conductance of the polyion λ_p can be written as the ratio of the total charge $Q_p = z_1 efN$ on the polyion chain to the total electrophoretic coefficient f_{Etot}.

$$\lambda_p = \mathcal{F}\mu_p = \mathcal{F}\frac{Q_p}{f_{Etot}}, \tag{71}$$

where $\mathcal{F} = e\mathcal{N}$ is the Faraday number, with $\mathcal{N}$ being the Avogadro number.

A polyion in dilute solution is surrounded by an oppositely charged atmosphere whose spatial distribution is distorted and becomes asymmetric in the presence of an external electric field. As a consequence, in calculating the electrophoretic coefficient, the effect of the resulting 'asymmetry field' must be summed up to the external electric field effect [160, 161].

According to Manning [122], the total electrophoretic coefficient f_{Etot}, corrected for the 'asymmetry field' effect, due to the distortion of the ionic atmosphere surrounding the polyion and acting as a field oppositely directed to the external electric field, can be written as

$$f_{Etot} = \left[f_E + \frac{Q_p}{\mu_1^0}\left(1 - \frac{D_1}{D_1^0}\right)\right]\frac{D_1^0}{D_1}, \tag{72}$$

where μ_1^0 is the counterion mobility in water (without polyions present) and f_E is the electrophoretic coefficient without the asymmetry field correction.

The resulting equivalent polyion conductance λ_p is then given by [122]

$$\lambda_p = \left(\mathcal{F}Q_p\frac{D_1}{D_1^0}\right)\left[f_E + \frac{Q_p}{\mu_1^0}\left(1 - \frac{D_1}{D_1^0}\right)\right]^{-1}. \tag{73}$$

To obtain the coefficient f_E, a model for the chain is needed. To this end, if the polyion is considered as an ensemble of N_b simple, spherical, structural units (beads) of radius R_b, taking into account the effect due to hydrodynamic interactions, the electrophoretic coefficient can be written as [162, 163]

$$f_E = \frac{N_b \zeta_b}{1 + (\zeta_b/6\pi\eta N_b) \sum_i^{N_b} \sum_{j \neq i}^{N_b} \langle r_{ij}^{-1} \rangle}, \tag{74}$$

where $\zeta_b = 6\pi\eta R_b$ is the friction coefficient, with η being the viscosity of water and r_{ij} the distance between different structural units in the specified configuration.

In Manning's picture, the structural units are the effectively charged monomers (after condensation) on the polyion chain and the hydrodynamic interactions between them are mediated by the electrostatic interaction with the surrounding (oppositely charged) counterion atmosphere that, under the influence of the external field, drags the solvent in the opposite direction (charged solvent effect). Within this picture, hydrodynamic interactions between units that are further apart than a Debye length (r_D, equation (3)) are 'screened', while stretches of the chain of length comparable with r_D should be considered fully extended [122]. By introducing this assumption as an exponential cutoff, $\exp(-r_{ij}/r_D)$, within the double summation in the denominator of equation (74), this sum can be easily summed up and the electrophoretic friction coefficient calculated as [122]

$$f_E = \frac{N_b \zeta_b}{1 + (\zeta_b/3\pi\eta b)|\ln(b/r_D)|} \approx \frac{3\pi\eta N_b b}{|\ln(b/r_D)|}. \tag{75}$$

The final expression for the electrical conductivity of a salt-free polyelectrolyte solution in the presence of counterion condensation, within the Manning model [122], reads

$$\sigma = fc \frac{D_1}{D_1^0} \left\{ \lambda_1^0 + \left(\mathcal{F} z_1 e f N \frac{D_1}{D_1^0} \right) \left[\frac{z_1 e f N}{\mu_1^0} \left(1 - \frac{D_1}{D_1^0} \right) + \frac{3\pi\eta N_b b}{|\ln(b/r_D)|} \right]^{-1} \right\}. \tag{76}$$

5.1.1. Comparison with data in dilute solutions. Figure 12 shows clearly that the overlap concentration of high-molecular-weight polyelectrolyte solutions is very small (see equation (46)). This makes dilute aqueous polyelectrolyte solutions difficult to study, particularly in the salt-free limit. In an inert atmosphere, the fact that water dissociates to make 2×10^{-7} moles of small ions per litre of water puts a practical lower bound on the 'salt-free' concentrations. When the solution is exposed to air, this situation is even worse, because carbon dioxide reacts with water to form carbonic acid [164], which then dissociates to impart a small ion concentration of order of 4×10^{-6} moles of small ions per litre (the pH of ultra-pure water exposed to air is 5.4) [165]. Hence, for aqueous solutions exposed to air, there is a practical lower bound for 'salt-free' solutions of order 10^{-4} moles of charged monomers per litre.

Conductivity has been a primary means of characterizing polyelectrolyte solutions for many years [166]. Wandrey *et al* [123, 167–169] have recently made extensive use of the Manning model for conductivity of dilute polyelectrolyte solutions in inert atmospheres and compared the results with ion selective electrode measurements of counterion activity. Representative results are shown in figure 15, for solutions of poly(vinylbenzyltrialkylammonium) chloride of various chain lengths. Equivalent conductance is defined as

$$\Lambda = \frac{\sigma - \sigma_s}{c}, \tag{77}$$

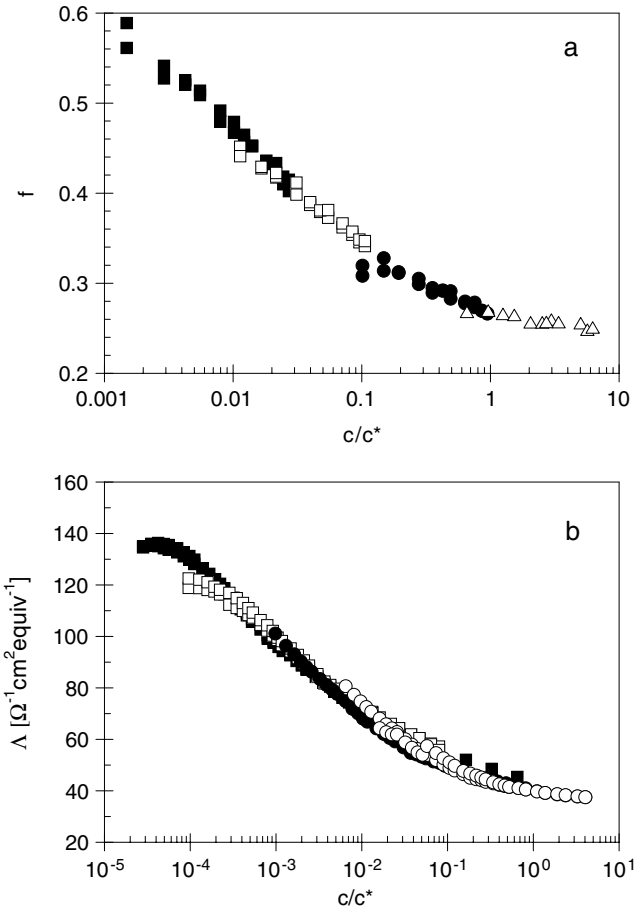

Figure 15. Counterion activity coefficient (a) and equivalent conductance (b) of poly(vinylbenzyltrialkylammonium) chloride aqueous solutions ($N = 27$ are ■, $N = 56$ are □, $N = 142$ are △, $N = 181$ are ● and $N = 407$ are ○). Data are from [168].

where σ_s is the conductivity of the solvent. The counterion activity coefficient and equivalent conductance both increase as the concentration is lowered below the overlap concentration c^* because the entropy of dissociation grows as the concentration is lowered [120, 135, 170, 171].

5.2. Scaling models for semi-dilute solutions

The Manning model has been recently extended, for flexible polyelectrolytes and in the absence of added salt, to finite concentration systems (dilute and semi-dilute regimes) [43, 125, 172] on the basis of the scaling picture for the chain conformation of a polyelectrolyte in solution [119, 128–131]. Scaling concepts, successfully used for uncharged polymers, have been applied to the description of the chain conformation of polyelectrolyte solutions in different conformation regimes by de Gennes *et al* [135, 173], Odijk [170], Grosberg and Khokhlov [128] and, more recently, by Rubinstein and co-workers [119, 129–131]. In this picture (see section 3.2), a polyion can be represented as a chain of 'electrostatic blobs', with the statistics of the chain inside the blob determined by the thermodynamic interaction between uncharged

polymer and solvent. The number of monomers and the number of condensed counterions inside an electrostatic blob, i.e., the effective charge, and the blob size are determined by a balance between polymer–solvent and electrostatic interactions inside the blob [119, 129–131].

At very low concentration, in the dilute regime with no added salt, the Debye screening length (equation (3)) is much larger than the distance between chains and charges interact via the unscreened Coulomb potential. The polymer chain is represented by a highly extended configuration of N/g_e electrostatic blobs of size ξ_e. Each electrostatic blob contains g_e monomers and bears an effective electric charge $z_1 efg_e$ (f is the fraction of 'free' counterions) of order unity. Any effect of counterion condensation is incorporated into the concept of the electrostatic blob [129, 130].

Following the derivation of Manning, the elementary unit that contributes to the overall friction coefficient is the electrostatic blob. The friction coefficient of a fully extended (rod-like) configuration of N/g_e beads of size ξ_e can be calculated as [43, 174]

$$f_E = \frac{3\pi\eta N\xi_e}{g_e \ln(N/g_e)}, \tag{78}$$

which is the same result obtained by Manning (equation (75)) except that now the 'structural units' are the electrostatic blobs (not single monomers) and the assumption of an electrostatic cutoff length for hydrodynamic interactions (r_D) is not needed anymore.

Hence, the full expression for the electrical conductivity in dilute solutions and in a good solvent condition reads [43, 124]

$$\sigma = fc\frac{D_1}{D_1^0}\left\{\lambda_1^0 + \left(\mathcal{F}z_1 efN\frac{D_1}{D_1^0}\right)\left[\frac{z_1 efN}{\mu_1^0}\left(1-\frac{D_1}{D_1^0}\right) + \frac{3\pi\eta N\xi_e}{g_e\ln(N/g_e)}\right]^{-1}\right\} \quad \text{dilute solution.} \tag{79}$$

In semi-dilute solutions, the polyion chain is modelled as a random walk of N/g correlation blobs of size ξ, each of them containing g monomers. Each correlation blob bears an electric charge $z_1 efg$ and the whole chain, of contour length $L = N\xi/g$, bears a charge $Q_p = z_1 efN$.

Due to the strong electrostatic interactions within each correlation blob, the chain is an extended assembly of electrostatic blobs inside the correlation volume (for $r < \xi$). For $r > \xi$, electrostatic and hydrodynamic interactions are screened and the chain is a random walk of correlation blobs of size ξ [129, 130]. The 'structural unit' that should be used in calculating the friction coefficient (equation (74)) is the correlation blob. Taking into account the asymmetry field effect [122, 160, 161], the friction coefficient for a random coil [163] of N/g statistical units of length ξ is given by

$$f_E = \frac{N\zeta_\xi/g}{1+\frac{8}{3}\sqrt{N/g}(\zeta_\xi/\sqrt{6\pi^3}\eta\xi)}, \tag{80}$$

where the friction coefficient ζ_ξ of a correlation blob can be easily calculated, in analogy to equation (78), as

$$\zeta_\xi = \frac{3\pi\eta\xi}{\ln(g/g_e)}, \tag{81}$$

since, within a correlation blob, the chain is a fully extended configuration of g/g_e electrostatic blobs of size $\xi_e = \xi/(g/g_e)$. The polyion equivalent conductance is obtained by combining equations (73) and (80).

$$\lambda_p = \left(\mathcal{F}z_1 efN\frac{D_1}{D_1^0}\right)\left[\frac{z_1 efN}{\mu_1^0}\left(1-\frac{D_1}{D_1^0}\right) + \frac{N\zeta_\xi/g}{1+\frac{8}{3}\sqrt{N/g}(\zeta_\xi/\sqrt{6\pi^3}\eta\xi)}\right]^{-1}. \tag{82}$$

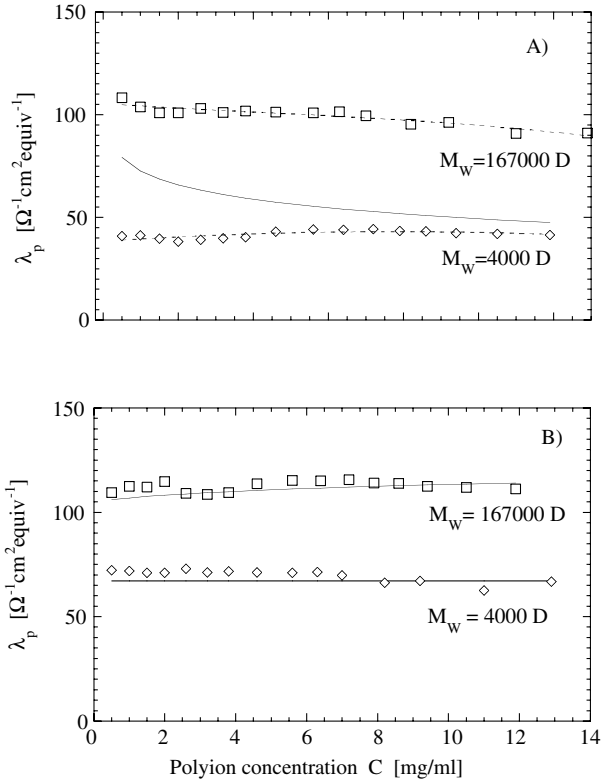

Figure 16. Comparison between predicted and observed polyion equivalent conductances λ_p for poly(L-lysine) at $T = 30\,^{\circ}$C. The polyion concentrations investigated are below the overlap concentration c^* for the lower molecular weight ($M_w = 4000$ is ◇) and above c^* for the higher one ($M_w = 167\,000$ is □) [43]. (A) An equivalent conductance λ_p predicted by the Manning model (equation (73), ——) assuming Manning condensation with $f = b/l_B = 0.48$ and the values calculated from the measured conductivity σ within the same model (equation (76)). (B) An equivalent conductance λ_p calculated from the measured conductivity within the scaling approach in the appropriate dilute (equation (79)) and semi-dilute (equation (83)) regimes. The solid lines represent fits, with f used as a concentation-independent adjustable parameter, in the two different concentration regimes. For the $M_w = 4000$ sample, the line is equation (79) with $f = 0.67$ and, for the $M_w = 167\,000$ sample, the line is equation (83) with $f = 0.39$.

In this case, for good solvent conditions, the full expression for electrical conductivity in semi-dilute solutions is written as [43, 124]

$$\sigma = fc\frac{D_1}{D_1^0}\left\{\lambda_1^0 + \left(\mathcal{F}z_1 efN\frac{D_1}{D_1^0}\right)\left[\frac{z_1 efN}{\mu_1^0}\left(1-\frac{D_1}{D_1^0}\right) + \frac{N\zeta_\xi/g}{1+\frac{8}{3}\sqrt{N/g}(\zeta_\xi/\sqrt{6\pi^3}\eta\xi)}\right]^{-1}\right\} \qquad \text{semi-dilute solution,} \tag{83}$$

with ζ_ξ given by equation (81).

A comparison between the Manning model and the prediction of the scaling model for semi-dilute polyelectrolyte solutions is shown in figure 16. Here, the counterion contribution to conductivity has been subtracted, using each model, to provide the equivalent conductance from the polyion, λ_p. Such data are shown for two poly(L-lysine) samples [43] with $M_w = 4000$ and 167 000. The Manning model predicts that the polyion equivalent conductance is independent

of molecular weight [122] and, hence, there is a single prediction based on equations (73) and (76) shown as the solid line in figure 16(A). The line curves because the Debye length depends on concentration (see equation (76)) and this prediction does not agree with either data set, although the high concentration data for the dilute sample (with $M_w = 4000$) are reasonably well predicted. The fact that the Manning model fails for the $M_w = 167\,000$ data is hardly surprising, since these data are all above c^*, while the Manning model assumes dilute solution. However, the failure of the Manning model for the $M_w = 4000$ data is noteworthy since these data are all below c^*. Figure 16(B) compares predictions and data from conductivity within the scaling model (equations (79) and (83)) considering counterion condensation. The dependence on molecular weight and concentration are markedly improved when the scaling approach is used to describe the chain conformation. λ_p is predicted and observed to be independent of polyion concentration in dilute solution (equation (79)) and adopts a very weak concentration dependence in semi-dilute solution (equation (83)). The slight increase in λ_p on dilution in dilute solution likely reflects the increase of f due to the increased entropy of free counterions, seen more clearly in figure 15.

Under poor solvent conditions, the configuration of the polyelectrolyte chain can be better described in terms of the 'necklace globule' model [119, 131]. In this model, the competition between the strong hydrophobic polymer–solvent interactions and the electrostatic repulsion creates an electrostatic instability (analogous to the Rayleigh breakup of a charged drop) that forces the local conformation of the polyelectrolyte into a sequence of charged globules (beads), connected by more elongated stretches of the chain (strings).

In the dilute regime, the electrostatic screening length is much larger than the distances between chains and larger than the whole necklace length. The 'structural unit' in the Manning picture is now 'a bead plus a string', with l_s the string length, D_b the bead diameter and with $D_b \ll l_s$. Assuming that the friction is concentrated in the beads and following the Manning derivation (equations (74)–(75)) with the exponential cutoff which is now equal to the total length of the necklace $L = N_b l_s$, the friction coefficient reads [125]

$$f_E = \frac{3\pi\eta N_b D_b}{1 + (D_b/l_s)|\ln(N_b)|}. \tag{84}$$

In the semi-dilute regime, two different conditions are possible. When, in the lower concentration range, the condition $l_s < \xi < L$ on the correlation length ξ holds (the 'string controlled' semi-dilute regime), the electrophoretic coefficient is given by equation (80), but with the friction coefficient ζ_ξ written as [125]

$$\zeta_\xi = \frac{3\pi\eta N_b D_b}{1 + (D_b/l_s)|\ln(l_s/\xi)|}. \tag{85}$$

At higher concentrations, where $L \gg \xi \approx l_s$ (the 'bead controlled' semi-dilute regime), the friction coefficient ζ of the correlation length reduces to the friction coefficient of a single bead and it is hence given by [125]

$$\zeta_\xi = 3\pi\eta D_b. \tag{86}$$

Again, substituting back in the expression for the electrophoretic coefficient f_E (equation (80)) the appropriate friction coefficient ζ_ξ (equation (85) or (86)), and proceeding backward in the usual way, the complete expression for the electrical conductivity of the solution is obtained.

Colby *et al* [172] proposed that the asymmetry field could be safely neglected in a semi-dilute solution, since polarization in neighbouring correlation volumes should have offsetting

effects. In the absence of added salt, the conductivity of a semi-dilute polyelectrolyte solution could be described by considering a polyion equivalent conductance

$$\lambda_p = \frac{\mathcal{F} z_1 efg \ln(g/g_e)}{3\pi\eta\xi}. \tag{87}$$

This leads directly to a simple prediction for the conductivity of semi-dilute polyelectrolyte solutions neglecting the asymmetry field effect [172].

$$\sigma = fc\left(\lambda_1^0 + \frac{\mathcal{F} z_1 efg \ln(g/g_e)}{3\pi\eta\xi}\right) \qquad \text{semi-dilute solution.} \tag{88}$$

The two predictions for conductivity of semi-dilute polyelectrolyte solutions, either including (equation (83)) or omitting (equation (88)) the asymmetry field effect, have been compared with experimental data and found to give satisfactory descriptions [124]. A computer simulation of polyelectrolyte conductivity would be particularly useful in deciding whether either of these predictions are robust.

6. Conclusions and outlook

Dielectric and conductometric methods have enormous potential for characterizing the effective charge of polyelectrolyte chains in solution. However, that potential has not yet been fully realized for dielectric methods. Figure 17 compares the fraction of monomers bearing an effective charge determined by conductivity (equation (88)), dielectric spectroscopy (equation (57)) and osmotic pressure π. The latter estimates f from

$$f = \frac{1.8\pi}{ckT}, \tag{89}$$

where the prefactor of 1.8 was chosen to match the f determined from conductivity measurements (whereas the Katchalsky cell model [6] expects this coefficient to be 2). Figure 17 shows that the agreement between osmotic pressure and conductivity is within the small uncertainties in each technique, for semi-dilute solutions of NaPSS and NaPAMS, with no added salt. This is important, as it means that *the scaling models for conductivity can be used to calculate f and that value can be expected to agree with the f from osmotic pressure* within a prefactor of order unity. The upturn in apparent f at high concentrations has been suggested to be caused by release of counterions from the polyelectrolyte, owing to the increased dielectric constant of the medium when strongly charged polyions (with many condensed counterions) are present in significant concentrations in water [25]. However, the Katchalsky cell model also predicts a similar upturn in osmotic coefficient at high concentrations [175–177].

While conductivity is relatively simple and easy to interpret in terms of the effective charge, dielectric results have thus far been less reliable. The f calculated from the intermediate frequency dielectric relaxation in semi-dilute solution (equation (57)) shows considerabe scatter. The dielectric determinations of f are also considerably larger than those from osmotic pressure or conductivity, but this is as expected, since scaling models have been utilized which ignore prefactors of order unity. The dielectric determinations of f could be divided by a factor of 2 or 3 to bring them in better agreement with the other determinations. Unfortunately, the large scatter in those data preclude any robust conclusions from the comparison plot. The scatter originates from the difficulties in isolating the intermediate frequency relaxation from the relaxations at higher and lower frequencies, as discussed in section 2.2. Only through systematic experimentation can trends be isolated, and our recent work [25] (squares in figure 17) suggests that the trend observed by dielectric spectroscopy in the concentration

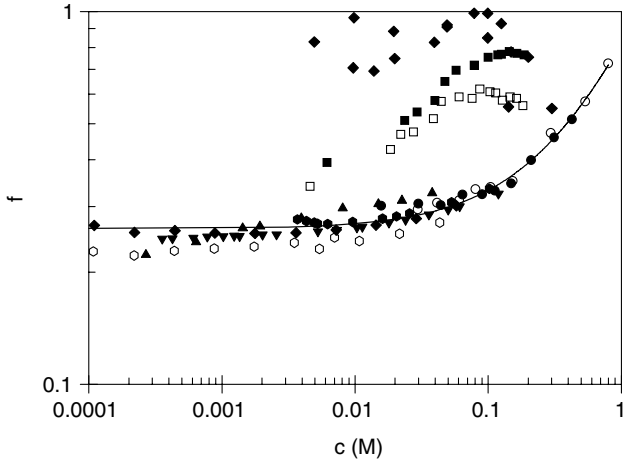

Figure 17. Concentration dependence of effective charge for the sodium salts of two sulfonated polyelectrolytes: open symbols are NaPAMS and filled symbols are NaPSS. Data are from osmotic pressure results using equation (89) ((○, ●) [180] and (△, ▲) [181]); upside-down triangles [182] and hexagons [172] are from conductivity measurements using equation (88); squares [25] and diamonds [22] are from the intermediate frequency dielectric relaxation in semi-dilute solution using equation (57).

dependence of effective charge may differ from that reported previously by osmotic pressure and conductivity.

The current situation for analysis of the low-frequency dielectric dispersion is even worse. More data are desperately needed to guide the development of theory for the low-frequency relaxation.

The contributions of dipoles along the chain, either due to polar side chains or counterions condensed on the polyion, should have a dielectric relaxation somewhere in the interesting range of frequencies. Such relaxations, along with the relaxation of bound water, may well interfere with both the intermediate and low-frequency relaxations. Understanding such relaxations may be essential before dielectric methods can be used routinely to determine effective charge on polyelectrolytes in solution. The dielectric methods are powerful, as they determine two parameters (a dielectric increment and a relaxation time scale). The dielectric increment can be used to determine the solvent quality in a poor solvent [25] or to unambiguously identify good solvent conditions [26]. However, interpretation of dielectric measurements is simply not at the level of the simple conductivity measurements.

More work needs to be done to develop models for interpreting conductometric and dielectric measurements on polyelectrolyte solutions. Computer simulations would be helpful in guiding that theoretical effort to better understand the molecular aspects of polarization at different frequencies. Monte Carlo simulations are currently underway [178] but molecular dynamics simulations with an explicit solvent are not quite possible yet [179].

Appendix. Dielectric parameters of the NaCl solutions to be used as standard solutions

The parameters $\varepsilon_w, \varepsilon_\infty, \tau_{H_2O}, \sigma_0$ that appear in equation (31) can be easily calculated for NaCl solutions at the different molarities and temperatures by means of the following polynomials, with the coefficients given in table A.1 [71].

Table A.1. Coefficients of the polynomials for calculating the dielectric parameters of NaCl solutions, as a function of NaCl concentration and temperature [71].

$t_0 = 87.74$; $t_1 = -4.0008\ \mathrm{K}^{-1}$; $t_2 = 0.0009398\ \mathrm{K}^{-2}$; $t_3 = 1.41 \times 10^{-6}\ \mathrm{K}^{-3}$
$c_1 = -0.2551\ \mathrm{l\,mol}^{-1}$; $c_2 = 0.05151\ \mathrm{l}^2\ \mathrm{mol}^{-2}$; $c_3 = -0.006889\ \mathrm{l}^3\ \mathrm{mol}^{-3}$
$a_0 = 1.1109 \times 10^{-10}$ s; $a_1 = -3.824 \times 10^{-12}\ \mathrm{K}^{-1}$ s; $a_2 = 6.938 \times 10^{-14}\ \mathrm{K}^{-2}$ s; $a_3 = -5.096 \times 10^{-16}\ \mathrm{K}^{-3}$ s
$b_1 = 0.001463\ \mathrm{K}^{-1}\ \mathrm{l\,mol}^{-1}$; $b_2 = -0.04896\ \mathrm{l\,mol}^{-1}$; $b_3 = -0.02967\ \mathrm{l}^2\ \mathrm{mol}^{-2}$; $b_4 = 0.005644\ \mathrm{l}^3\ \mathrm{mol}^{3}$
$s_{c1} = 10.394\ \mathrm{l\,mol}^{-1}$; $s_{c2} = -2.3776\ \mathrm{l}^2\ \mathrm{mol}^{-2}$; $s_{c3} = 0.68258\ \mathrm{l}^3\ \mathrm{mol}^{-3}$;
$s_{c4} = -0.13538\ \mathrm{l}^4\ \mathrm{mol}^{-4}$; $s_{c5} = 0.010086\ \mathrm{l}^5\ \mathrm{mol}^{-5}$
$s_{t1} = 3.02 \times 10^{-5}\ \mathrm{S\,m}^{-2}\ \mathrm{K}^{-1}\ \mathrm{l\,mol}^{-1}$; $s_{t2} = 3.922 \times 10^{-5}\ \mathrm{S\,m}^{-2}\ \mathrm{K}^{-2}\ \mathrm{l\,mol}^{-1}$;
$s_{t3} = 1.721 \times 10^{-5}\ \mathrm{S\,m}^{-2}\ \mathrm{K}^{-1}\ \mathrm{l}^2\ \mathrm{mol}^{-2}$; $s_{t4} = -6.584 \times 10^{-6}\ \mathrm{S\,m}^{-2}\ \mathrm{K}^{-2}\ \mathrm{l}^2\ \mathrm{mol}^{-2}$
$s_1 = -0.01962\ \mathrm{K}^{-1}$; $s_2 = 8.08 \times 10^{-5}\ \mathrm{K}^{-2}$

Static dielectric permittivity ε_w:

$$\varepsilon_w = \varepsilon_{w1}[1 + c_1C + c_2C^2 + c_3C^3], \tag{A.1}$$

where ε_{w1} is given by

$$\varepsilon_{w1} = t_0 + t_1T + t_2T^2 + t_3T^3. \tag{A.2}$$

T is the temperature in centigrade, C is the concentration in mol l^{-1}.

Relaxation time $\tau_{\mathrm{H_2O}}$:

$$\tau_{\mathrm{H_2O}} = \tau_1[1 + b_1CT + b_2C + b_3C^2 + b_4C^3] \tag{A.3}$$

with τ_1 defined as

$$\tau_1 = \frac{1}{2\pi}[a_0 + a_1T + a_2T^2 + a_3T^3]. \tag{A.4}$$

Conductivity σ:

$$\sigma = \sigma_c[1 - \sigma_t + s_1\Delta T + s_2(\Delta T)^2], \tag{A.5}$$

where $\Delta T = 25 - T$, and σ_t and σ_c are given by

$$\sigma_t = s_{t1}\Delta TC + s_{t2}(\Delta T)^2C + s_{t3}\Delta TC^2 + s_{t4}(\Delta T)^2C^2, \tag{A.6}$$

$$\sigma_c = s_{c1}C + s_{c2}C^2 + s_{c3}C^3 + s_{c4}C^4 + s_{c5}C^5. \tag{A.7}$$

References

[1] Hasted J 1973 *Aqueous Dielectrics* (London: Chapman and Hall)
[2] Grant E H, Sheppard R J and South G P 1978 *Dielectric Behaviour of Biological Molecules in Solutions* (Oxford: Clarendon)
[3] Takashima S 1989 *Electrical Properties of Biopolymers and Membranes* (Philadelphia: Institute of Physics Publishing)
[4] Feldman Y, Zuev Y, Polygalov E and Fedotov V 1992 *Colloid Polym. Sci.* **270** 768
[5] Oosawa F 1971 *Polyelectrolytes* (New York: Dekker)
[6] Katchalsky A 1971 *Pure Appl. Chem.* **26** 327
[7] Mandel M and Odijk T 1984 *Annu. Rev. Phys. Chem.* **35** 75
[8] Schmitz K S 1993 *Macroions in Solution and Colloidal Suspension* (New York: VCH)
[9] Forster S and Schmidt M 1995 *Adv. Polym. Sci.* **120** 51–133
[10] Barrat J-L and Joanny J-F 1996 Theory of polyelectrolyte solutions *Adv. Chem. Phys.* vol 94 (New York: Wiley)
[11] Mandel M 1999 *Physical Properties of Polyelectrolyte Solutions* (Firenze, Italy: Pacini Editore)
[12] Block H and North A M 1970 *Adv. Mol. Relax. Processes* **1** 309
[13] Manning G S 1969 *J. Chem. Phys.* **51** 934
[14] Manning G S 1979 *Acc. Chem. Res.* **12** 443

[15] Buchner R, Barthel J and Stauber J 1999 *Chem. Phys. Lett.* **306** 57
[16] Kaatze U, Behrends R and Pottel R 2002 *J. Non-Cryst. Solids* **305** 19
[17] Arkhipov V I 2002 *J. Non-Cryst. Solids* **305** 127
[18] van der Touw F and Mandel M 1974 *Biophys. Chem.* **2** 218
[19] Vreudgenhil T, van der Touw F and Mandel M 1979 *Biophys. Chem.* **10** 67
[20] van Dijk W, van der Touw F and Mandel M 1981 *Macromolecules* **14** 792
[21] van Dijk W, van der Touw F and Mandel M 1981 *Macromolecules* **14** 1554
[22] Ito K, Yagi A, Ookubo N and Hayakawa R 1990 *Macromolecules* **23** 857
[23] Nagamine I, Ito K and Hayakawa R 1999 *Langmuir* **15** 4135
[24] Nagamine I, Ito K and Hayakawa R 1999 *Colloids Surf.* A **148** 149–53
[25] Bordi F, Cametti C, Tan J S, Boris D C, Krause W E, Plucktaveesak N and Colby R H 2002 *Macromolecules* **35** 7031
[26] Bordi F, Cametti C, Gili T and Colby R H 2002 *Langmuir* **18** 6404
[27] Mashimo S, Miura N, Shinyahiki N and Ota T 1993 *Macromolecules* **26** 6859
[28] Mashimo S 1997 *Dielectric Spectroscopy of Polymeric Materials* ed J P Runt and J J Fitzgerald (Washington, DC: American Chemical Society)
[29] Bordi F, Cametti C and Paradossi G 1996 *Biopolymers* **40** 485
[30] Bordi F, Cametti C and Paradossi G 1999 *Phys. Chem. Chem. Phys.* **1** 1555
[31] Bordi F, Cametti C and Paradossi G 2000 *Biopolymers* **53** 129
[32] Williams G and Watts D C 1960 *Trans. Faraday Soc.* **66** 800
[33] Williams G, Watts D C, Dev S B and North M 1961 *Trans. Faraday Soc.* **67** 1323
[34] Lindsey C P and Patterson G D 1980 *J. Phys. Chem.* **73** 3348
[35] Alvarez F, Alegria A and Colmenero J 1993 *Phys. Rev.* B **47** 125
[36] Cole K S and Cole R H 1941 *J. Chem. Phys.* **9** 341
[37] Davidson D W and Cole R H 1950 *J. Chem. Phys.* **18** 1417
[38] Davidson D W 1961 *Can. J. Chem.* **39** 571
[39] Havriliak S and Negami S 1966 *J. Polym. Sci.* C **14** 99
[40] Böttcher C J F and Bordewijk P 1978 *Theory of Electric Polarization* vol 2 (Amsterdam: Elsevier)
[41] Fytas G and Anastasiadis S H 1994 *Disorder Effects on Relaxational Processes* ed R Richeart and A Blumen (Berlin: Springer)
[42] Adachi K and Kotaka T 1988 *Macromolecules* **21** 157
[43] Bordi F, Cametti C, Motta A and Paradossi G 1999 *J. Phys. Chem.* B **103** 5092
[44] Bordi F and Cametti C 2001 *J. Colloid Interface Sci.* **237** 224
[45] Schwarz G 1972 *Adv. Mol. Relax. Processes* **3** 281
[46] Takashima S, Gabriel G, Sheppard R J and Grant E H 1984 *Biophys. J.* **46** 29
[47] Takashima S 1967 *Biopolymers* **5** 899
[48] Bonincontro A, Cametti C, Di Biasio A and Pedone F 1984 *Biophys. J.* **45** 495
[49] Mandel M 2000 *Biophys. Chem.* **85** 125
[50] Feldman Y, Nigmatullin R, Polygalov E and Texter J 1998 *Phys. Rev.* E **58** 7561
[51] Feldman Y, Skodvin T and Sjöblom J 2001 Dielectric spectroscopy on emulsion and related colloidal systems. A review *Encyclopedic Handbook of Emulsion Technology* ed J Sjöblom (New York: Marcel-Dekker)
[52] Lee S B, Smith R L, Inomata H and Arai K 2000 *Rev. Sci. Instrum.* **71** 4226
[53] Fannin P C, Perova T S, Giannitis A T, Nolan M, Moore A R and Gamble H S 2001 *J. Mater. Sci.: Mater. Electron.* **12** 347
[54] Asami K 2002 *Prog. Polym. Sci.* **27** 1617
[55] van der Touw F, Selier G and Mandel M 1975 *J. Phys. E: Sci. Instrum.* **8** 844
[56] Blom J 1979 *J. Phys. E: Sci. Instrum.* **12** 889
[57] Bottomley P A 1978 *J. Phys. E: Sci. Instrum.* **11** 413
[58] Mandel M and Jenard A 1958 *Bull. Soc. Chim. Belg.* **67** 575
[59] Federigi N L and Barbenza G H 1974 *J. Phys. E: Sci. Instrum.* **7** 719
[60] Bianco B, Drago G P, Marchesi M, Martini C, Mela G and Ridell S 1979 *IEEE Trans. Instrum. Meas.* **IM-28** 290
[61] Essex C G, South G P, Sheppard R J and Grant E H 1975 *J. Phys. E: Sci. Instrum.* **8** 385
[62] van Beek W M, van der Touw F and Mandel M 1976 *J. Phys. E: Sci. Instrum.* **9** 385
[63] Yonekura T 1994 *Hewlett-Packard J.* **45** 67
[64] Yonekura T 1994 *Proc. 1994 IEEE Conf. on Instrumentation and Measurement Technology (Shizuoka, Japan)*
[65] van der Touw F, de Goede J, van Beek W M and Mandel M 1975 *J. Phys. E: Sci. Instrum.* **8** 840
[66] Rosen D, Bignal R, Wisse J D M and van der Drift A C M 1969 *J. Phys. E: Sci. Instrum.* **2** 22

[67] Takashima S, Casaleggio A, Giuliano F, Morando M, Arrigo P and Ridell S 1986 *Biophys. J.* **49** 1003
[68] Sachs S B, Katchalsky A and Spiegler K S 1970 *Electrochim. Acta* **15** 693
[69] Jackson J D 1999 *Classical Electrodynamics* 3rd edn (New York: Wiley)
[70] Schwan H P and Maczuk J 1960 *Rev. Sci. Instrum.* **31** 59
[71] Stogryn A 1971 *IEEE Trans. Microwave Theory Tech.* **MTT-19** 733
[72] Havriliak J S and Havriliak S I 1997 *Dielectric and Mechanical Relaxation in Materials* (New York: Hanser Publisher)
[73] Bordi F, Cametti C and Motta A 2000 *Macromolecules* **33** 1910
[74] Warburg E 1899 *Ann. Phys. Chem.* **67** 493
[75] Mandel M 1956 *Bull. Soc. Chim. Belg.* **65** 305
[76] Chassagne C, Bedeaux D, van der Ploeg J P M and Koper G J M 2002 *Colloids Surf.* A **210** 137
[77] Cirkel P A, van der Ploeg J P M and Koper G J M 1997 *Physica* A **235** 269
[78] Schwan H P and Ferris C D 1968 *Rev. Sci. Instrum.* **39** 481
[79] Tamamushi R and Takahashi K 1974 *Electroanal. Chem. Interf. Electrochem.* **50** 277
[80] Wakamatsu H 1997 *Hewlett-Packard J.* **48** 37
[81] Ong K G, Wang J, Singh R S, Bachas L G and Grimes C A 2001 *Biosensors Bioelectron.* **16** 305
[82] Fricke H and Curtis H J 1937 *J. Phys. Chem.* **41** 729
[83] Schwan H P 1963 Determination of biological impedances *Physical Techniques in Biological Research* vol VI, part B, ed W Nastuk (New York: Academic)
[84] Takashima S 1963 *J. Polym. Sci.* A **1** 2791
[85] Shaw T M 1942 *J. Chem. Phys.* **10** 609
[86] van der Touw F and Mandel M 1971 *Trans. Faraday Soc.* **67** 1336
[87] van der Touw F, Mandel M, Honijk D D and Verhoog H G F 1971 *Trans. Faraday Soc.* **67** 1343
[88] Oncley J L 1938 *J. Am. Chem. Soc.* **60** 1115
[89] Davey C L, Markx G H and Kell D 1990 *Eur. Biophys. J.* **18** 255
[90] Takashima S 1966 *J. Phys. Chem.* **70** 1372
[91] Raicu V, Saibara T and Irimajiri A 1998 *Bioelectrochem. Bioenerg.* **47** 325
[92] Maruska H P and Stevens J G 1988 *IEEE Trans. Electr. Insul.* **23** 197
[93] de Levie R 1965 *Electrochim. Acta* **10** 113
[94] de Levie R 1989 *J. Electroanal. Chem.* **261** 1
[95] Bordi F, Cametti C and Gili T 2001 *Bioelectrochemistry* **54** 53
[96] Wang J C 1988 *Electrochim. Acta* **33** 707
[97] Nyikos L and Pajkossy T 1985 *Electrochim. Acta* **30** 1533
[98] Pajkossy T and Nyikos L 1992 *J. Electroanal. Chem.* **332** 55
[99] Wang J C 1989 *Electrochim. Acta* **34** 987
[100] Cao Q, Wong P and Schwartz L M 1994 *Phys. Rev.* B **50** 5771
[101] Kerner Z and Pajkossy T 2000 *Electrochim. Acta* **46** 207
[102] Sadkowski A, Motheo A J and Neves R S 1998 *J. Electroanal. Chem.* **455** 107
[103] ChangHee K, SuIl P and JongHuy K 2003 *Electrochim. Acta* **48** 3455
[104] Hara M 1993 *Polyelectrolytes* (New York: Dekker)
[105] Schmitz K S 1993 *Macroions in Solution and Colloidal Suspension* (New York: VCH)
[106] Dautzenberg W J, Kotz B P, Seidel C and Stcherbina D 1994 *Polyelectrolytes: Formation, Characterization, Application* (Munich: Hanser)
[107] Imai N and Onishi J 1959 *Chem. Phys.* **30** 1115
[108] Minakata A, Imai N and Oosawa F 1972 *Biopolymers* **11** 347
[109] Oosawa F 1970 *Biopolymers* **9** 677
[110] Oosawa F 1958 *J. Polym. Sci.* **XXIII** 421
[111] Manning G S 1969 *J. Chem. Phys.* **51** 924
[112] Manning G S 1972 *Annu. Rev. Phys. Chem.* **23** 117
[113] Manning G S 1996 *Physica* A **231** 236
[114] Stigter D 1995 *Biophys. J.* **69** 380
[115] Deserno M, Holm C and May S 2000 *Macromolecules* **33** 199
[116] Kholodenko A and Beyerlein L 1995 *Phys. Rev. Lett.* **74** 4679
[117] Ramanathan G V and Woodbury C P 1982 *J. Chem. Phys.* **77** 4133
[118] Le Bret M and Zimm B H 1984 *Biopolymers* **23** 287
[119] Dobrynin A V and Rubinstein M 2001 *Macromolecules* **34** 1964
[120] Deshkovski A, Obukhov S and Rubinstein M 2001 *Phys. Rev. Lett.* **86** 2341
[121] Shklovskii B I 1999 *Phys. Rev. Lett.* **82** 3268

[122] Manning G S 1981 *J. Phys. Chem.* **85** 1506
[123] Wandrey C 1999 *Langmuir* **15** 4069
[124] Bordi F, Colby R H, Cametti C, De Lorenzo L and Gili T 2002 *J. Phys. Chem.* B **106** 6887
[125] Bordi F, Cametti C and Gili T 2002 *Phys. Rev.* E **66** 021803
[126] Popov A and Hoagland D A 2004 *J. Polym. Sci.: Polym. Phys.* **42** 3616
[127] Muthukumar M 2004 *J. Chem. Phys.* **120** 9343
[128] Grosberg A Y and Khokhlov A R 1994 *Statistical Physics of Macromolecules* (New York: AIP Press)
[129] Rubinstein M, Colby R H and Dobrynin A V 1994 *Phys. Rev. Lett.* **73** 2776
[130] Dobrynin A V, Colby R H and Rubinstein M 1995 *Macromolecules* **28** 1859
[131] Dobrynin A V and Rubinstein M 1999 *Macromolecules* **32** 915
[132] Manning G S 1970 *Biopolymers* **9** 1543
[133] Manning G S 1975 *J. Phys. Chem.* **79** 262
[134] Manning G S 1984 *J. Phys. Chem.* **88** 6654
[135] de Gennes P G, Pincus P, Velasco R M and Brochard F J 1976 *J. Phys. (France)* **37** 1461
[136] Nierlich M *et al* 1979 *J. Phys. (France)* **40** 701
[137] Khokhlov A R 1980 *J. Phys. A: Math. Gen.* **13** 979–87
[138] Dobrynin A V, Rubinstein M and Obukhov S P 1996 *Macromolecules* **29** 2974
[139] Schiessel H and Pincus P 1998 *Macromolecules* **31** 7953–59
[140] Limbach H J and Holm C 2003 *J. Phys. Chem.* B **107** 8041
[141] Agmon N 1996 *J. Phys. Chem.* **100** 1072
[142] Shinyashiki N, Yagihara S, Arita I and Mashimo S 1998 *J. Phys. Chem.* B **102** 3249
[143] Ryabov Y E, Feldman Y, Shinyashiki N and Yagihara S 2002 *J. Chem. Phys.* **116** 8610
[144] Jacobson B 1955 *J. Am. Chem. Soc.* **77** 2919
[145] Dukhin S S and Shilov V N 1974 *Dielectric Phenomena and the Double Layer in Disperse Systems and Polyelectrolytes* (New York: Wiley)
[146] Dukhin S S and Derjaguin B V 1974 Equilibrium double layer and electrokinetic phenomena *Surface and Colloid Science* vol 7, ed E Matijevic (New York: Wiley)
[147] Fixman M 1980 *J. Chem. Phys.* **72** 5177
[148] Fixman M 1980 *Macromolecules* **13** 711
[149] Fixman M 1981 *J. Chem. Phys.* **75** 4040
[150] Fixman M and Jagannathan S 1981 *J. Chem. Phys.* **75** 4048
[151] Ookubo N, Hirai Y, Ito K and Hayakawa R 1989 *Macromolecules* **22** 1359
[152] Boris D C and Colby R H 1998 *Macromolecules* **31** 5746
[153] Kaji K, Urakawa H, Kanaya T and Kitamaru R 1988 *J. Phys. (France)* **49** 993
[154] Oostwal M G, Blees M H, de Bleijser J and Leyte J C 1993 *Macromolecules* **26** 7300
[155] Nierlich M, Boue F, Lapp A and Oberthur R 1985 *J. Phys. (France)* **46** 649
[156] Takahashi Y, Matsumoto N, Iio S, Kondo H and Noda I 1999 *Langmuir* **15** 4120
[157] Prabhu V M, Muthukumar M, Wignall G D and Melnichenko Y B 2001 *Polymer* **42** 8935
[158] Krause W E, Tan J S and Colby R H 1999 *J. Polym. Sci.: Polym. Phys.* **37** 3429
[159] Ander P and Kardan M 1984 *Macromolecules* **17** 2436
[160] Schmitt A, Meullenet J P and Varoqui R 1978 *Biopolymers* **17** 413
[161] Schmitt A, Meullenet J P and Varoqui R 1978 *Biopolymers* **17** 1249
[162] Kirkwood J K and Riseman J 1948 *J. Chem. Phys.* **16** 565
[163] Kirkwood J K and Riseman J 1954 *J. Polym. Sci.* **12** 1
[164] Shedlovsky T and MacInnes D A 1935 *J. Am. Chem. Soc.* **57** 1705
[165] Cohen J, Priel Z and Rabin Y 1988 *J. Chem. Phys.* **88** 7111
[166] Eisenberg H 1958 *J. Polym. Sci.* **30** 47
[167] Wandrey C 1996 *Ber. Bunsenges. Phys. Chem.* **100** 869
[168] Wandrey C, Hunkeler D, Wendler U and Jaeger W 2000 *Macromolecules* **33** 7136
[169] Wandrey C and Hunkeler D 2002 Study of polyion counterion interaction by electrochemical methods *Handbook of Polyelectrolytes and their Applications* ed S K Tripathy, J Kumar and H S Nalwa (Stevenson Ranch: American Scientific)
[170] Odijk T 1979 *Macromolecules* **12** 688
[171] Liao Q, Dobrynin A V and Rubinstein M 2003 *Macromolecules* **36** 3399
[172] Colby R H, Boris D C, Krause W E and Tan J S 1997 *J. Polym. Sci.: Polym. Phys.* **35** 2951
[173] de Gennes P G 1980 *Scaling Concepts in Polymer Physics* (Ithaca, NY: Cornell University Press)
[174] Dhont J K G 1996 *An Introduction to Dynamics of Colloids* (New York: Elsevier)
[175] Marcus R A 1955 *J. Chem. Phys.* **23** 1057

[176] Katchalsky A, Alexandrowicz Z and Kedem O 1966 Polyelectrolyte solutions *Chemical Physics of Ionic Solutions* ed B E Conway and R G Barradas (New York: Wiley)
[177] Deserno M and Holm C 2001 Cell model and Poisson–Boltzmann theory: a brief introduction *Electrostatic Effects in Soft Matter and Biophysics* ed C Holm, P Kekicheff and R Podgornik (Boston: Kluwer)
[178] Washizu H and Kikuchi K 2002 *J. Phys. Chem.* B **106** 11329
[179] Levy R M and Gallicchio E 1998 *Annu. Rev. Phys. Chem.* **49** 531
[180] Essafi W 1996 Structure des polyelectrolytes fortement charges, PhD Thesis, Universite Pierre et Marie Curie, Paris
[181] Takahashi A, Kato T and Nagasawa M 1970 *J. Phys. Chem.* **74** 944
[182] Kwak J C T and Hayes R C 1975 *J. Phys. Chem.* **79** 265